

# Crossover between BCS Superconductor and Doped Mott Insulator of $d$ -wave Pairing State in Two-Dimensional Hubbard Model

Hisatoshi YOKOYAMA<sup>\*</sup>, Masao OGATA<sup>1</sup>, Yukio TANAKA<sup>2</sup>, Kenji KOBAYASHI<sup>3</sup>,  
and Hiroki TSUCHIURA<sup>4</sup>

*Department of Physics, Tohoku University, Sendai 980-8578, Japan*

<sup>1</sup>*Department of Physics, University of Tokyo, Bunkyo-ku, Tokyo 113-0033, Japan*

<sup>2</sup>*Department of Applied Physics, Nagoya University, Nagoya 464-8603, Japan*

<sup>3</sup>*Department of Natural Science, Chiba Institute of Technology, Narashino 275-0023, Japan*

<sup>4</sup>*Department of Applied Physics, Tohoku University, Sendai 980-8579 Japan*

With high- $T_c$  cuprates in mind, properties of correlated  $d_{x^2-y^2}$ -wave superconducting (SC) and antiferromagnetic (AF) states are studied for the Hubbard ( $t$ - $t'$ - $U$ ) model on square lattices, using a variational Monte Carlo method. We employ simple trial wave functions including only crucial parameters, such as a doublon-holon binding factor indispensable to describe correlated SC and normal states as doped Mott insulators.  $U/t$ ,  $t'/t$  and  $\delta$  (doping rate) dependence of relevant quantities are systematically calculated. As  $U/t$  increases, a sharp crossover of SC properties occurs at  $U_{co}/t \sim 10$  from a conventional BCS type to a kinetic-energy-driven type for any  $t'/t$ . As  $\delta$  decreases,  $U_{co}/t$  is smoothly connected to the Mott transition point at half filling. For  $U/t \lesssim 5$ , steady superconductivity corresponding to the cuprates is not found, whereas the  $d$ -wave SC correlation function  $P_d^\infty$  rapidly increases for  $U/t \gtrsim 6$  and becomes maximum at  $U = U_{co}$ . Comparing the  $\delta$  dependence of  $P_d^\infty$  with experimentally observed dome-shaped  $T_c$  and condensation energy, we find that the effective value of  $U$  for the cuprates should be larger than the band width, for which the  $t$ - $J$  model is valid. Analyzing the kinetic energy, we reveal that for  $U > U_{co}$  only doped holes (electrons) become charge carriers, which will make a small Fermi surface (hole pocket), but for  $U < U_{co}$  all the electrons (holes) contribute to conduction and will make an ordinary large Fermi surface, which is contradictory to the feature of cuprates. By introducing a proper negative (positive)  $t'/t$ , the SC (AF) state is stabilized. In the underdoped regime, the strength of SC for  $U > U_{co}$  is determined by two factors, i.e., the AF spin correlation, which creates singlet pairs (pseudogap), and the charge mobility dominated by Mott physics. In this connection, we argue that the electrons near the antinodal points in the momentum space play a leading role to stabilize the  $d$ -wave state, contrary to the dichotomy of electronic roles in the momentum space proposed for the two-gap problem. We also show the instability of the hole-doped AF state against phase separation.

**KEYWORDS:** superconductivity, cuprate, antiferromagnetism, pseudogap, doped Mott insulator, doublon-holon binding, Hubbard model, strong correlation, variational Monte Carlo method.

## 1. Introduction

The essence of superconductivity (SC) in the high- $T_c$  cuprates is most probably captured by two-dimensional (2D)  $t$ - $J$  and Hubbard models;<sup>1,2)</sup> a variety of theories have been developed on the basis of these models.<sup>3-5)</sup> In the ground state of the  $t$ - $J$ -type models, which deal with strongly correlated regimes, different approaches concluded that superconducting (SC) states with  $d_{x^2-y^2}$ -wave symmetry are stabilized in the parameter range relevant to the cuprates, as we will see further in §2.1. Meanwhile, approaches starting from the weak-correlation limit<sup>6,7)</sup> of the Hubbard model provided complementary, but often qualitative, views of SC for the cuprates, particularly in thermal and dynamical properties. Nevertheless, quantum Monte Carlo (QMC) methods,<sup>8-10)</sup> quantitatively reliable approaches for finite correlation strengths, unanimously yielded a result that the SC correlation function never develops in weakly correlated regimes as compared with the noninteracting case, and therefore cast a serious doubt on the ground of the weak-correlation theories for applying them to realistic

correlation strengths. Thus, it is important to clarify how properties of a  $d_{x^2-y^2}$ -wave SC state evolve as the correlation strength is increased in the Hubbard model.

To this end, the variational Monte Carlo (VMC) method<sup>11,12)</sup> is useful for its continuous applicability from weakly to strongly correlated regimes in a quantitative manner. This is by virtue of correct treatment of the local electron correlations. Since the early stage of research in the cuprates, VMC studies<sup>13-15)</sup> have mainly treated  $t$ - $J$ -type models and yielded results basically consistent with the behavior of cuprates.<sup>5)</sup> Later, the present authors have studied a many-body SC state, applying it to the 2D Hubbard ( $t$ - $t'$ - $U$ ) model [ $U$ : onsite Coulomb correlation,  $t$ ,  $t'$ : hopping integrals to the nearest-neighbor (NN) and diagonal sites].<sup>16-19)</sup> In refs. 16 (for  $t' = 0$ ) and 17, we discussed superconductor (SC)-insulator (Mott) transitions at half filling arising at  $U = U_c \sim 7t$  without directly introducing an AF correlation. According to these and recent studies,<sup>20,21)</sup> a binding effect between a doubly occupied site (doublon, D) and an empty site (holon, H) plays a leading role in nonmagnetic Mott transitions. Ref. 16 also showed for doped cases that a sharp crossover exists at  $U = U_{co} \sim W$

[ $W(=8t)$ : band width], where the nature of the  $d_{x^2-y^2}$ -wave SC state,  $\Psi_Q^d$ , changes qualitatively from a usual BCS type for  $U < U_{co}$  to an unconventional strongly correlated type for  $U > U_{co}$ , in which  $\Psi_Q^d$  is stabilized by the reduction in kinetic energy. This crossover for SC is smoothly connected to the Mott transition at half filling ( $U_{co} \rightarrow U_c$ ), as the doping rate  $\delta$  is decreased. Thus, the strongly correlated SC state for  $U > U_{co}$  deserves a doped Mott insulators,<sup>22)</sup> and will be deeply influenced by the effect of D-H binding correlation.

In this paper, as a development of refs. 16 and 17, we study SC and antiferromagnetism (AF) independently for doped cases by systematically changing the values of  $U/t$ ,  $t'/t$  and  $\delta$ , using D-H binding wave functions. The primary purpose is to establish that the nature of SC is qualitatively different between the regimes of  $U < U_{co}$  and  $U > U_{co}$  by studying various quantities, and that the behavior of cuprates is contradictory to that of  $d$ -wave BCS-type SC realized for  $U < U_{co}$  in various aspects, but consistent with the behavior of doped Mott insulators ( $U > U_{co}$ ).

The second purpose of this paper is to consider a differentiation or dichotomy of electronic roles in the momentum space,<sup>23,24)</sup> in connection with the pseudogap problem. Early experimental studies in the so-called two-gap problem<sup>25-28)</sup> posed a question on a familiar view that the pseudogap stems from incoherent pairs of electrons<sup>29-32)</sup> for  $T_c < T < T^*$ . Two characteristic energy scales (gaps) were discovered whose  $\delta$ -dependences are mutually opposite in the underdoped regime. They seemed to stem from the electrons with wave numbers near the nodal ( $\pi/2, \pi/2$ ) and antinodal ( $\pi, 0$ ) points, and correspond to the SC gap and pseudogap, respectively, indicating that the origin of the pseudogap is not directly connected to pairing. Recent experiments for the pseudogap have taken on more complicated aspects,<sup>33-40)</sup> and are still actively developing.<sup>41,42)</sup> In this study, we argue that the two energy scales are interpreted as a pairing gap and its correction by the charge fluctuation released from a Mott insulating state. And that the electronic states near the antinodal point ( $\pi, 0$ ) [not in the nodal region  $\sim (\pi/2, \pi/2)$ ] are crucial to the  $d$ -wave SC.<sup>32,43)</sup>

A part of the results were reported previously.<sup>44,45)</sup>

The rest of this paper is organized as follows: In §2, we explain the model and method used in this paper. In §3, we present the results for  $t' = 0$  to grasp basic features of  $U/t$  and  $\delta$  dependence of relevant quantities, and argue the existence of a crossover and its relevance to cuprates. In §4, we discuss the effects of diagonal transfer  $t'$ , which provides a clue for understanding the stability of SC and AF states. In §5, we argue that the electrons near the antinodal point play a leading role to realize the  $d$ -wave SC. In §6, the main results are summarized. In Appendix A, we give supplementary explanations of the model. In Appendix B, we compare some forms of doublon-holon binding factors as a supplement to §2.2. In Appendix C, we describe in detail the definition and justification of the long-distance value of  $d$ -wave pair correlation function in the present cases.

## 2. Formalism

In §2.1, we explain the Hubbard model and the background of this study. In §2.2, we introduce many-body trial wave functions used in this paper. In §2.3, we briefly summarize the setting of VMC calculations.

### 2.1 Hubbard Model for Cuprates

As a model of the  $\text{CuO}_2$  planes, we consider the Hubbard model on a square lattice:

$$\begin{aligned}\mathcal{H} &= \mathcal{H}_{\text{kin}} + \mathcal{H}_U \\ &= \sum_{\mathbf{k}\sigma} \varepsilon(\mathbf{k}) c_{\mathbf{k}\sigma}^\dagger c_{\mathbf{k}\sigma} + U \sum_j d_j,\end{aligned}\quad (1)$$

with  $d_j = n_{j\uparrow}n_{j\downarrow}$  (doublon projector) and  $n_{j\sigma} = c_{j\sigma}^\dagger c_{j\sigma}$ . Although the band structure  $\varepsilon(\mathbf{k})$  is qualitatively important,<sup>46-52)</sup> we consider, for clarity, only the minimum terms to distinguish material dependence i.e., NN ( $t$ ) and diagonal-neighbor ( $t'$ ) hoppings:

$$\varepsilon(\mathbf{k}) = -2t(\cos k_x + \cos k_y) - 4t' \cos k_x \cos k_y. \quad (2)$$

We use  $t$  and the lattice constant as the units of energy and length, respectively. As discussed in Appendix A, the effective onsite repulsion  $U/t$  may differ between electron-doped and hole-doped cases. For the ease of calculations, we can restrict the electron density to  $n = N/N_s \leq 1$  ( $N$ : electron number;  $N_s$ : site number), or the doping rate to  $\delta = 1 - n \geq 0$  by a canonical transformation. Then,  $t'/t$  becomes negative (positive) for hole-(electron-)doped cases (see Appendix A).

The studies of this model for the cuprates are roughly classified into weak- and strong-correlation theories. In the former,<sup>6)</sup> stability and some properties of  $d_{x^2-y^2}$ -wave SC are discussed, using RPA,<sup>53)</sup> FLEX approximations,<sup>54)</sup> renormalization-group<sup>7)</sup> and perturbative<sup>55,56)</sup> approaches. As we will show in §3 and §4, however, no substantial enhancement of the SC correlation function appropriate for the high- $T_c$  cuprates is found in a weak-correlation regime ( $U/t \lesssim 5$ ). Such a result is not restricted to our studies. Early QMC studies<sup>8)</sup> drew negative conclusions for the appearance of SC in the weak-coupling regime ( $U/t = 2-4$ ). A recent QMC study<sup>9)</sup> using an expansion with Gaussian bases also obtained a negative result for SC in the overdoped regime up to  $U/t = 7$  for  $t' = 0$ . Another recent study<sup>10)</sup> concluded that the  $d_{x^2-y^2}$ -wave pair susceptibility is not enhanced for  $t' = 0$ , but a SC Kosteritz-Thouless transition exists for moderately large  $U/t$ 's and  $t'/t = -0.2$ . Thus, it is improbable that the small- $U/t$  Hubbard model with  $t' = 0$  gives such a sufficiently high  $T_c$  as the cuprates display; a doubt arise as to the reliability of the weak-correlation theories for the cuprates, at least in a quantitative sense. In this connection, we will check whether or not the introduction of  $t'/t$  term can enhance SC in the weak correlation regime.

In the strong-correlation limit, the Hubbard model is mapped to  $t$ - $J$ -type models, in which robust  $d_{x^2-y^2}$ -wave SC is found by VMC,<sup>13-15)</sup> exact diagonalization,<sup>57)</sup> a projector Monte Carlo methods,<sup>58)</sup> besides by various mean-field-type approximations.<sup>4,5)</sup> In the correspond-

ing large- $U/t$  regime of the Hubbard model, firm  $d$ -wave SC and its competition with AF orders were found near half filling by VMC studies<sup>59–61</sup> using trial functions similar to ours.<sup>16–19</sup> Another promising quantitative method to treat this regime is extensions of the dynamical mean field theory (DMFT). First, using a dynamical cluster approximation, a finite temperature instability to  $d$ -wave SC was found.<sup>62</sup> Subsequently, the stability of  $d$ -wave SC and the competition with AF were studied using different variations of DMFT.<sup>63–65</sup> As far as we know, there are no theories that reliably drew negative results for SC in this regime. It seems appropriate to assume that robust  $d_{x^2-y^2}$ -wave SC corresponding to the high- $T_c$  cuprates is realized in the Hubbard model with  $U \gtrsim W$  near half filling.

Finally, we touch on the coexistence of  $d$ -wave SC and AF long-range orders. This problem has been repeatedly addressed for the 2D  $t$ - $J$  and Hubbard models, using e.g. VMC methods<sup>59, 66, 67</sup> and DMFT.<sup>63, 68</sup> These studies found the stability of coexisting states against both pure  $d$ -wave and AF states near half filling; other studies<sup>65, 69, 70</sup> showed that such mixing states appear for small  $\delta$  only under certain conditions. Experimentally, explicit evidence of microscopic coexistence has not been discovered for most high- $T_c$  cuprates,<sup>71</sup> except for multilayered Hg systems.<sup>72–74</sup> It is probable that the coexistence can be realized in clean  $\text{CuO}_2$  plains in the multilayered systems, while the absence of the coexistence in usual cases will be due to disorder. Meanwhile, inhomogeneous phases such as stripe<sup>75</sup> can compete or coexist with the  $d_{x^2-y^2}$  wave SC.<sup>41, 42, 76</sup> Anyway, as a basis to tackle complicated states, it is vital to study the pure  $d$ -wave and AF states separately and their competition.

## 2.2 Variational wave functions

We implement a series of VMC calculations. Removing irrelevant variational parameters, we elucidate basic behaviors of simple correlated  $d$ -wave SC and AF wave functions of the Jastrow type,<sup>77</sup>

$$\Psi = \mathcal{P}\Phi, \quad (3)$$

when it is applied to the Hubbard model, eq. (1). Here,  $\mathcal{P}$  denotes a many-body correlation (Jastrow) factor composed of projection operators, and  $\Phi$  a one-body (mean-field) wave function given by a Slater determinant.

In the many-body part, we consider two projection operators:  $\mathcal{P} = \mathcal{P}_Q \mathcal{P}_G$ .<sup>16, 17</sup> Although the onsite repulsive (Gutzwiller) projector,<sup>78</sup>

$$\mathcal{P}_G = \prod_j [1 - (1 - g)d_j], \quad (4)$$

with  $0 \leq g \leq 1$  is of primary importance, intersite correlation factors are indispensable for a qualitatively correct description of Hubbard-type models.<sup>79</sup> Among them, an attractive factor between a doublon and a holon is crucial at half filling, which is defined as,<sup>80, 81</sup>

$$\mathcal{P}_Q = \prod_j (1 - Q_j), \quad (5)$$

where  $Q_j (=Q_j^S)$  is a D-H projector of the site  $j$ :

$$Q_j^S = \mu \left[ d_j \prod_{\tau} (1 - h_{j+\tau}) + h_j \prod_{\tau} (1 - d_{j+\tau}) \right]. \quad (6)$$

Here,  $h_j = (1 - n_{j\uparrow})(1 - n_{j\downarrow})$ , and  $\tau$  runs over all the NN sites of the site  $j$ . The projector  $\mathcal{P}_Q$  with  $Q_j^S$  yields  $(1 - \mu)^{N_D + N_H}$ , if isolated  $N_D$  doublons and  $N_H$  holons exist in the electron configuration, where an isolated doublon (holon) indicates a doublon (holon) not accompanied by holons (doublons) in its four NN sites. The parameter  $\mu$  ( $\leq 1$ ) controls the strength of D-H correlation; for  $\mu = 1$ , a doublon and a holon are completely bound in mutually NN sites, for  $\mu = 0$ , they are completely free, and for  $\mu < 0$ , they become repulsive to one another. As we repeatedly showed,  $\mathcal{P}_Q$  or its analog plays a leading role to induce conductor(metal)-to-nonmagnetic-insulator (Mott) transitions<sup>17, 20, 21, 82</sup> and spin-gap transitions in attractive Hubbard models.<sup>83, 84</sup> Recent studies using more elaborate long-range D-H factors<sup>20, 21</sup> showed that the simplest NN form  $Q_j^S$  works unexpectedly well. We use this form  $Q_j^S$  for  $\delta = 0$  in this study. We found that a D-H correlation factor is still important for  $\delta \neq 0$ ,<sup>16</sup> if  $\delta$  is roughly within the range of SC for the cuprates. A NN D-H pair yields, with a single hopping process, an antiparallel-spin pair, which contributes to the pairing in  $d$ -wave SC. Because the symmetry between a doublon and a holon is broken for  $\delta \neq 0$ , an asymmetric form of  $Q_j$  seems reasonable. Thus, for  $\delta > 0$ , we use a simple asymmetric form:

$$Q_j = Q_j^D = \mu d_j \prod_{\tau} (1 - h_{j+\tau}), \quad (7)$$

for the ease of calculations. In Appendix B, we check different forms of  $Q_j$  in detail. The main conclusion is that the details of  $Q_j$  makes no difference at least qualitatively; a simple form of  $Q_j$  like eq. (7) preserves the essence of the D-H binding mechanism. In §3.1, we will discuss the condition that the D-H binding factor becomes significant.

For the frustrated cases ( $t' \neq 0$ ), D-H correlation between diagonal sites may also play a certain role. Therefore, we similarly introduce a D-H projector  $Q'_j$  with a variational parameter  $\mu'$  for inter-diagonal sites. Eventually, the D-H factor for  $t' \neq 0$  becomes

$$\mathcal{P}_Q = \prod_j (1 - Q_j) (1 - Q'_j). \quad (8)$$

In most calculations for  $t' = 0$ , we fixed  $\mu'$  at zero, because the optimized value of  $\mu'$  is small and the energy gain thereof is very small ( $\sim 10^{-4}t$  even for large  $U/t$ ).<sup>85</sup>

Now, we turn to the one-body function  $\Phi$  in eq. (3). As a continuation of the preceding papers, we mainly study a fixed- $N$   $d_{x^2-y^2}$ -wave singlet (BCS) state,  $\Phi_d(\Delta_d, \zeta)$ :<sup>86</sup>

$$\Phi_d = \left( \sum_{\mathbf{k}} a_{\mathbf{k}} c_{\mathbf{k}\uparrow}^{\dagger} c_{-\mathbf{k}\downarrow}^{\dagger} \right)^{\frac{N}{2}} |0\rangle, \quad (9)$$

with

$$a_{\mathbf{k}} = \frac{v_{\mathbf{k}}}{\omega_{\mathbf{k}}} = \frac{\Delta_{\mathbf{k}}}{\sqrt{\epsilon_{\mathbf{k}}^2 + \Delta_{\mathbf{k}}^2}}, \quad (10)$$

where  $\zeta$  is a variational parameter which is reduced to the chemical potential for  $U/t \rightarrow 0$ . Since it is known that the  $d_{x^2-y^2}$ -wave is the most stable among various gap shapes near half filling,<sup>13,14)</sup> here we exclusively treat the basic  $d_{x^2-y^2}$ -wave gap:<sup>87-91)</sup>

$$\Delta_{\mathbf{k}} = \Delta_d(\cos k_x - \cos k_y). \quad (11)$$

We should emphasize that, even if the variational parameter  $\Delta_d$  indicates the magnitude of the  $d$ -wave singlet gap, a many-body state ( $\Psi^d = \mathcal{P}\Phi_d$ ) with finite  $\Delta_d$  does not necessarily mean a SC state.<sup>92,93)</sup> To confirm the SC order, one needs to calculate the order parameter<sup>13)</sup> or pair correlation functions like  $P_d(\mathbf{r})$  introduced later. For  $\Delta_d = 0$ ,  $\Phi_d$  is reduced to the Fermi sea,  $\Phi_F$ ; in this paper, we use  $\Psi^F (= \mathcal{P}\Phi_F)$  as the reference normal state for the energy gain by  $\Delta_d$  (or  $\Delta_{AF}$ ). Furthermore, we fix the value of  $t'/t$  in  $\varepsilon_{\mathbf{k}}$  in the wave functions [eq. (10)] at the same value as that in the Hamiltonian, eq. (2), namely we do not explicitly introduce a band renormalization effect due to correlation. Because the renormalization of  $\varepsilon_{\mathbf{k}}$ <sup>94)</sup> brings about a serious effect in the vicinity of half filling,<sup>95)</sup> we will treat this issue in upcoming publications. As  $n$  goes away from half filling, the renormalization effect rapidly becomes modest.<sup>51,88)</sup>

In this paper, we consider a correlated AF-ordered state  $\Psi_Q^{AF} (= \mathcal{P}\Phi_{AF})$  independently of the  $d$ -wave state; as a one-body state, we use a Hartree-Fock solution on the square lattice,  $\Phi_{AF}(\Delta_{AF})$ :<sup>96)</sup>

$$\Phi_{AF} = \prod_{\mathbf{k}} \alpha_{\mathbf{k}\uparrow}^\dagger \prod_{\mathbf{k}} \alpha_{\mathbf{k}\downarrow}^\dagger, \quad (12)$$

with

$$\alpha_{\mathbf{k}\sigma}^\dagger = u_{\mathbf{k}} c_{\mathbf{k}\sigma}^\dagger + \text{sgn}(\sigma) v_{\mathbf{k}} c_{\mathbf{k}+\mathbf{Q}\sigma}^\dagger, \quad (13)$$

where  $\text{sgn}(\sigma) = 1$  or  $-1$  according as  $\sigma = \uparrow$  or  $\downarrow$ ,  $\mathbf{Q}$  is the AF nesting vector  $(\pi, \pi)$ , and

$$u_{\mathbf{k}}(v_{\mathbf{k}}) = \sqrt{\frac{1}{2} \left[ 1 - (+) \frac{\gamma_{\mathbf{k}}}{\sqrt{\gamma_{\mathbf{k}}^2 + \Delta_{AF}^2}} \right]}, \quad (14)$$

with  $\gamma_{\mathbf{k}} = -2t(\cos k_x + \cos k_y)$ . In the products of eq. (12), we take  $\mathbf{k}$ -points in the Fermi sea determined by  $\varepsilon_{\mathbf{k}}$  for convenience of optimization; namely, we do not allow for a band renormalization, similarly to  $\Phi_d$ .

### 2.3 Condition of VMC calculations

In optimizing parameters, we employ a simple method that repeatedly applies one-dimensional minimization (Brent method) to every parameter<sup>97)</sup> with the others fixed, because the number of parameters is small ( $\leq 6$ ). In most cases, the parameters as well as energy converge in a few iteration loops except for special cases near Mott transitions. To reduce the statistical errors, we continue the iteration loops for more 15-20 rounds after the convergence, and average the data accumulated in this additional process. In each loop, we use  $2.5 \times 10^5$  (typical)- $10^6$  fixed samples; consequently, the results in optimization are substantially averages of several million samples, with typical precision of the parameters and energy being the order of  $10^{-3}$  and  $10^{-4}t$ , respectively. In the calculations

of physical quantities using the optimized parameter sets, we averaged at least  $2.5 \times 10^5$  samples.

To check system-size dependence, we use systems of  $N_s = L \times L$  sites typically with  $L = 10$ -16, imposing on the periodic( $x$ )-antiperiodic( $y$ ) boundary conditions to reduce level degeneracy. In principle, we aim to satisfy the closed-shell condition, because open-shell systems bring about serious finite-size effects for small  $U/t$ 's, especially in the SC correlation function. However, when we treat  $t'/t$  dependence with other parameters fixed, we are obliged to use systems with open shells in addition to those with closed shells. In this connection, as we vary  $t'/t$ , the manner of  $\mathbf{k}$ -point occupation in  $\Phi$ , especially in  $\Phi_{AF}$  and  $\Phi_F$ , undergoes discontinuous changes at the values of  $t'/t$  specific to the system size. Consequently, large and irregular system-size dependence on  $t'/t$  occurs in most quantities even for large- $U/t$  cases, as we will encounter in §4. At any rate, we managed not to be affected by special cases by checking different systems.

### 3. Properties for $t' = 0$

We discuss the results for  $t' = 0$  first to grasp  $U/t$  and  $\delta$  dependence of various quantities. In §3.1, we consider the relation of the D-H binding to the Mott physics. In §3.2, by analyzing energies, we study the crossover of SC properties, competition between SC and AF, and instability of the AF state against phase separation. In §3.3, we consider the  $U/t$ -dependence of correlation functions. In §3.4, we argue that, in the underdoped regime,  $\delta$  dependence is different between the quantities derived from pairing and those from charge itinerancy, and that the strength of SC is represented by their product. In §3.5, a change in the mechanism of conduction is discussed.

#### 3.1 Relation of D-H binding to Mott physics

In Fig. 2 in ref. 16, we showed that the D-H binding correlation is highly effective for large values of  $U/t$  and small doping rates. Before discussing the main results, here we summarize this feature for  $t' = 0$ ; the feature for finite  $t'/t$ 's is basically the same as that for  $t' = 0$ .

Figure 1 shows the optimized D-H correlation parameter  $\mu$  [eqs. (6) and (7)]. Generally, as  $U/t$  increases,  $\mu$  increases, namely, the D-H binding becomes more tight, for the normal and SC states. The behavior near half filling is sharply distinguished according as  $U$  is smaller than  $U_c$  (Mott critical value) or not. For  $U < U_c$ ,  $\mu$  remains small ( $\mu \lesssim 0.5$ ), and decrease as  $L$  increases at  $\delta = 0$ , as indicated by an arrow, whereas for  $U > U_c$ ,  $\mu$  increases steadily as  $\delta$  decreases, abruptly approaches 1 for  $\delta \rightarrow 0$ , and increases as  $L$  increases. Thus,  $\mu$  still works for the Mott physics in doped systems. For the AF state, the D-H factor is redundant, as discussed in ref. 16; the redundancy is recognized from the behavior almost independent of  $\delta$  in Fig. 1.

The effect of the D-H factor is more clear in energy improvement. Figure 2(a) shows the difference of total energy per site ( $E$ ) between  $\Psi_Q^d = \mathcal{P}_Q \mathcal{P}_G \Phi_d$  ( $E_Q$ ) and  $\Psi_G^d = \mathcal{P}_G \Phi_d$  ( $E_G$ ). The energy gain by  $\mathcal{P}_Q$  increases as  $\delta$  decreases. For  $U < U_c$ , however, the gain remains small even at half filling (see also Table I). This feature is illustrated in Fig. 2(b) by  $U/t$  dependence of this

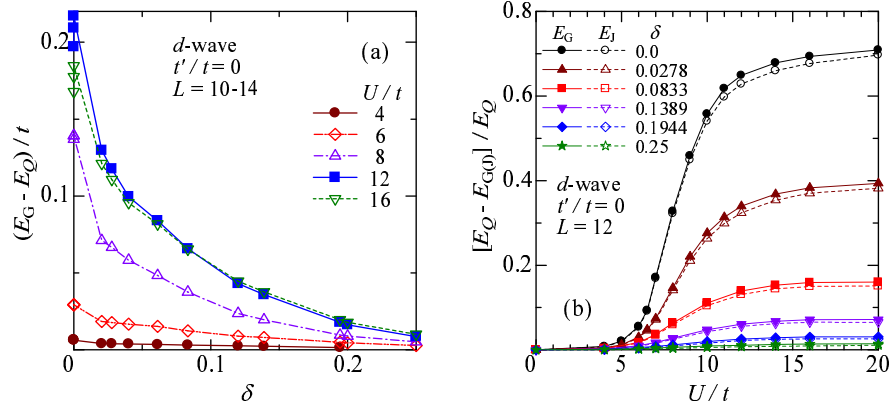


**Fig. 2.** (Color online) Improvement of energy by D-H binding factor on simple Gutzwiller projection for  $d$ -wave state. (a) Energy difference between  $\Psi_Q^d$  and  $\Psi_G^d$ , as function of doping rate for five  $U/t$ 's. (b) Energy difference between  $\Psi_Q^d$  and  $\Psi_G^d$  normalized by  $E_Q$  as function of  $U/t$  for six doping rates. The dashed lines with open symbols indicate the values obtained using  $\Psi_J^d$  instead of  $\Psi_Q^d$ .

**Table I.** The energy improvement by  $\Psi_Q^d$  and  $\Psi_J^d$  over  $E_G$  of  $\Psi_G^d$  in percent, i.e.,  $[E_{Q(J)} - E_G]/E_G \times 100$ , is listed for three values of  $U/t$  and of  $\delta$ .

$\delta$	$U/t \rightarrow$	4	8	12
0	$\Psi_Q$	0.81	48.7	184.9
	$\Psi_J$	0.08	0.7	5.8
0.083	$\Psi_Q$	0.33	17.1	16.1
	$\Psi_J$	0.06	0.5	0.9
0.194	$\Psi_Q$	0.15	2.8	2.6
	$\Psi_J$	0.08	0.2	0.4

the improvement is negligible for  $U/t \lesssim 5$ . In contrast, the energy gain becomes sizable for  $U \gtrsim U_c$ , where  $E$  is markedly improved by  $\mathcal{P}_Q$  at  $\delta = 0$  [Fig. 2(a)]. Although the energy gain by  $\mathcal{P}_Q$  decreases as  $\delta$  increases,  $\mathcal{P}_Q$  still brings appreciable improvement for  $0 \leq \delta \lesssim 0.15$ . This is roughly consistent with experiments in cuprates.<sup>98,99</sup> For large  $U/t$ 's, the contribution of  $\mathcal{P}_Q$  amounts to 2/3 of total  $E_Q$  at half filling, and preserves about 7% even for  $\delta \sim 0.15$ .

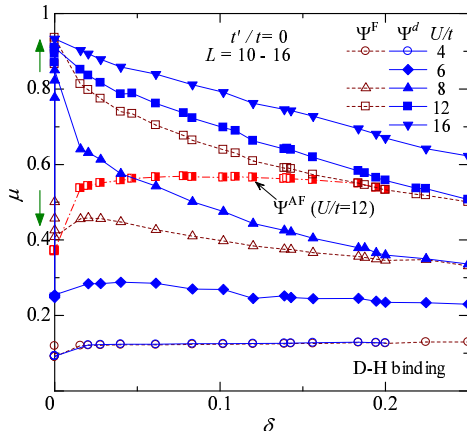


**Fig. 1.** (Color online) Optimized D-H binding parameter in the normal ( $\Psi_Q^F$ ),  $d$ -wave ( $\Psi_Q^d$ ), and antiferromagnetic ( $\Psi_Q^{AF}$ ) states as function of doping rate for some  $U/t$ 's. The arrows near the vertical axis indicate the difference of system-size dependence at  $\delta = 0$  between  $U > U_c$  and  $U < U_c$ . The data for  $L = 10-16$  are plotted together. The Mott transition points are estimated at  $U_c/t \sim 7$  and  $9$  for  $\Psi_Q^d$  and  $\Psi_Q^F$ , respectively.<sup>17)</sup>

The D-H binding correlation has a close relation to the spin exchange coupling, because a NN D-H pair yields a NN antiparallel spin pair with a single hopping. Correspondingly, the behavior of energy improvement in Figs. 2(a) and 2(b) becomes highly similar to that of the spin structure factor  $S(\mathbf{q})$  at  $\mathbf{q} = (\pi, \pi)$  as shown later in Figs. 14 and 10(a), respectively.<sup>45)</sup> Then, the effective range of  $\mathcal{P}_Q$  in the  $U/t$ - $\delta$  space coincides with the range of robust  $d$ -wave pairing [see  $\Delta_d$  as shown later in Figs. 11(a) and 5], because the  $d$ -wave pairing is mainly mediated by the AF spin correlation. Thus, the D-H binding correlation is crucial to the  $d$ -wave SC, and  $\Psi_Q^d$  literally represents a doped Mott insulator for  $U > U_c$ .

Having focused on attractive correlation as intersite factors, here we check that intersite repulsive correlation factors are irrelevant near half filling. For this purpose, we consider a typical NN repulsive Jastrow factor,

$$\mathcal{P}_J = \rho_D^{\hat{N}_{DD}} \rho_H^{\hat{N}_{HH}}, \quad (15)$$

with  $\rho_D$  and  $\rho_H$  being variational parameters, and

$$\hat{N}_{DD} = \sum_{j,\tau} d_j d_{j+\tau}, \quad \hat{N}_{HH} = \sum_{j,\tau} h_j h_{j+\tau}, \quad (16)$$

where  $j$  runs over all the lattice sites, and  $\tau$  NN sites of the site  $j$ . We compare improvement in energy by  $\Psi_J^d = \mathcal{P}_J \mathcal{P}_G \Phi_d (E_J)$  with that of  $\Psi_Q^d$  over  $E_G$  in Table I. In every case, the energy improvement by  $\Psi_J^d$  is much smaller than that by  $\Psi_Q^d$ . In Fig. 2(b), we plot  $(E_Q - E_J)/E_Q$  to compare with the case of  $E_G$ ; insignificance of  $\mathcal{P}_J$  is obvious in the present parameter regime. Long-range Jastrow factors are also considered irrelevant for  $\delta \sim 0$ , by inferring from the study at half filling.<sup>20,21)</sup> Henceforth, we disregard intersite repulsive factors.

### 3.2 Energy gain by $d$ -wave gap

Now, we consider SC properties. We begin with the energy gain ( $\Delta E$ ) by the  $d$ -wave gap parameter  $\Delta_d$ :

$$\Delta E = E(0) - E(\Delta_d^{\text{opt}}), \quad (17)$$

where  $E(\Delta_d)$  denotes the total energy for which the variational parameters other than  $\Delta_d$  are optimized, and

$\Delta_d^{\text{opt}}$  indicates the optimized value of  $\Delta_d$ . Although  $\Delta E$  has been often called “condensation energy”, we call it “energy gain” or “energy difference” in this paper, because  $\Delta E$  does not necessarily correspond to the SC condensation energy measured experimentally, as will be discussed in §3.4.

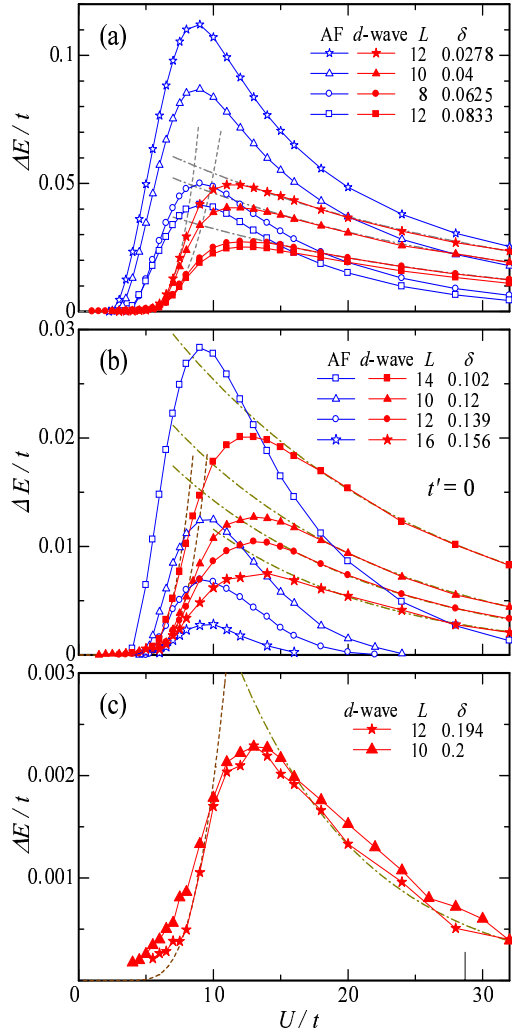


**Fig. 3.** (Color online)  $U/t$ -dependence of energy gain  $\Delta E/t$  for  $d$ -wave (solid symbols) and AF (open symbols) states for  $t' = 0$ . The three panels show different ranges of doping rates: (a) underdoped ( $0 < \delta < 0.1$ ), (b) lightly underdoped to optimum-doped ( $0.1 < \delta < 0.16$ ) and (c) over-doped ( $\delta \sim 0.2$ ) regimes. The AF state is not stabilize for  $\delta$ 's in (c). Note that energy scales are different among the panels. In each panel, the data of  $d$ -wave state are fitted with functions  $\alpha' \exp(-\beta' t/U)$  [dashed lines] in the weak-correlation side ( $U < U_{\text{co}}$ ) and  $\alpha \exp(-U/\beta t)$  [dash-dotted lines] in the strong-correlation side ( $U > U_{\text{co}}$ ).

Figure 3 shows the  $U/t$  dependence of  $\Delta E$  for the  $d$ -wave state ( $\Delta E^d$ ) and the AF state ( $\Delta E^{\text{AF}}$ ) defined for  $\Delta_{\text{AF}}$  similarly to eq. (17); the panels (a), (b) and (c) show the data for underdoped, optimum-doped, and over-doped values of  $\delta$ , respectively. As discussed in ref. 16,  $\Delta E^d$  is negligible for  $U \lesssim 6t$ , but abruptly increases as  $U/t$  increases, and is roughly fitted as  $\Delta E^d/t \sim \alpha' \exp(-\beta' t/U)^{100}$  at approximately  $U = W (= 8t)$  ( $\alpha'$ ,  $\beta'$ : constants).  $\Delta E^d$  has a maximum at  $U \sim U_{\text{co}} = 10t$ ,

then decreases slowly as fitted well with a curve,

$$\Delta E^d/t = \alpha \exp\left(-\frac{U}{\beta t}\right), \quad (18)$$

for  $2W \lesssim U < 4W$ . The estimated values of constants  $\alpha$  and  $\beta$  are shown in Fig. 4 as a function of  $\delta$ . From the form of eq. (18), we consider that the attractive pairing potential in this regime is proportional to  $t^2/U (= J/4)$ ; it indicates that the low-energy physics in this regime is parallel to that of the corresponding  $t$ - $J$ -type models.<sup>16,101</sup> Thus, we conclude that the properties of SC undergo a crossover from a BCS type to an unconventional  $t$ - $J$  type at  $U \sim U_{\text{co}}$  (This is a loose definition of  $U_{\text{co}}$ ). As long as  $\Psi_Q^d$  is SC, this behavior is qualitatively independent of  $\delta$ , although the magnitude of  $\Delta E^d$  decreases with  $\delta$ .

As obvious from the form of eq. (17),  $\Delta E^d$  originates from a finite  $d$ -wave gap. Actually, the behavior of  $\Delta E^d$  closely corresponds to that of the optimized  $\Delta_d$  shown in Fig. 5;  $\Delta_d$  abruptly starts to increase at  $U \sim U_c$ , where the D-H binding also becomes effective, as mentioned.

Now, we compare  $\Delta E^d$  with  $\Delta E^{\text{AF}}$ . As discussed in refs. 16 and 17,  $\Delta E^{\text{AF}}$  also has a maximum at  $U \sim W$  ( $U < U_{\text{co}}$ ) and has a tail for large  $U/t$ . At half filling,  $\Delta E^{\text{AF}}$  is always larger than  $\Delta E^d$  [Fig. 3 in ref. 16], although  $\Delta E^{\text{AF}}$  decreases rapidly for large  $U/t$ . Almost as

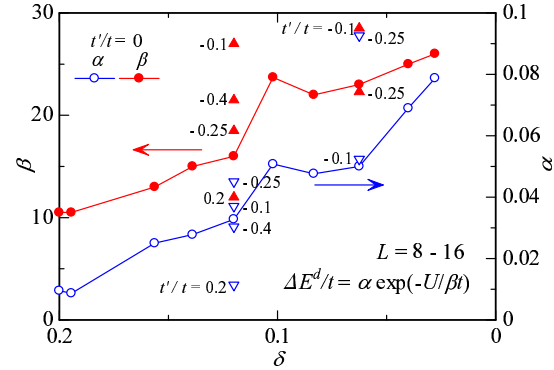


**Fig. 4.** (Color online) Coefficients  $\alpha$  (open symbols) and  $\beta$  (closed symbols) in fitting function of  $\Delta E^d/t$  for  $U > U_{\text{co}}$  [eq. (18)] as function of hole density. The circles denote the data for  $t' = 0$ . The data for  $t' \neq 0$  are included (triangles) with the values of  $t'/t$ .

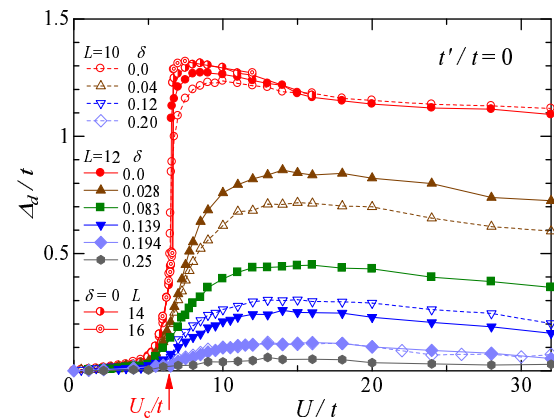


**Fig. 5.** (Color online) Optimized  $d$ -wave gap parameter in  $\Psi_Q^d$



soon as carriers are doped,  $\Delta E^{\text{AF}}$  is surpassed for large  $U/t$  [Fig. 3(a)], and tends to vanish at a certain value of  $U/t$  in the optimal-doped region [Fig. 3(b)]. As  $\delta$  increases,  $\Delta E^{\text{AF}}$  becomes smaller than  $\Delta E^d$  ( $\delta = 0.156$ ) for any value of  $U/t$ , and finally vanishes for  $\delta \sim 0.2$  [Fig. 3(c)]. The phase diagram constructed from these data [Fig. 4(a) in ref. 16] shows that the domain of  $d$ -wave SC tends to expand to  $\delta = 0$  and that of the AF state shrinks as  $U/W$  becomes large, supporting the result of the  $t$ - $J$  model, in which the stable state switches from an AF state to a  $d$ -wave state as soon as holes are doped.<sup>15)</sup> On the other hand, the AF state seems predominant at  $U \sim W$ . In fact, however, the AF domain in the phase diagram probably vanishes for  $\delta \neq 0$  (unless a  $d$ -wave SC order coexists<sup>67,70)</sup>) in accordance with the actual behavior of cuprates, because the AF state for a finite  $\delta$  is unstable against phase separation, as we will discuss shortly.

Let us turn to the behavior of components of  $\Delta E$ . In Figs. 6(a) and 6(b), the kinetic and interaction parts of  $\Delta E^d$  are shown as a function of  $U/t$ . For small  $U/t$  ( $\lesssim 10$ ), the energy gain is derived from the interaction part  $\Delta E_U$  with a loss in the kinetic part  $\Delta E_t$ . This mechanism is identical with that of the BCS theory. On the other hand, for large  $U/t$  ( $\gtrsim 12$ ), the SC state is stabilized by the reduction of  $\Delta E_t$ . As discussed in ref. 16, in this regime of  $U/t$ , the quasiparticle renormalization factor  $Z$  in the nodal direction is enhanced by introducing  $\Delta_d$ . This indicates that the SC coherence promotes the itinerancy of carriers, which is suppressed in the normal state by the strong correlation. Thus, we conclude that the so-called “kinetic-energy-driven SC” is realized only for  $U > U_{\text{co}}$ . A FLEX calculation for the Hubbard model also supports this behavior, although  $U_{\text{co}}/t$  is small and a sharp crossover is not obtained.<sup>102)</sup> Because  $E_t$  is proportional to the sum of optical conductivity  $\sigma_1(\omega)$  (exactly for  $t' = 0$ ),<sup>103)</sup> it is possible that precise optical measurements can determine whether or not the cuprates belong to the regime of the  $t$ - $J$  model.

Incidentally, similar behavior of  $\Delta E_U$  and  $\Delta E_t$  is found for the AF state as shown in Fig. 7, and for an  $s$ -wave SC state in the two-dimensional attractive Hubbard model.<sup>84)</sup> Accordingly, it is possibly a common tendency that nonorder-to-order transitions are induced by the reduction in kinetic energy in the strong-correlation regimes.<sup>104)</sup>

Finally, we discuss possible phase separation. This subject is important in relation to the density modulations or phase separation reported in the underdoped cuprates,<sup>105)</sup> and has been theoretically pursued mainly for the  $t$ - $J$  model with small  $J/t$ .<sup>106)</sup> A homogeneous state is unstable against phase separation if the charge compressibility,

$$\kappa = \frac{1}{n^2} \chi_c = \left( n^2 \frac{\partial^2 E}{\partial n^2} \right)^{-1}, \quad (19)$$

is negative, namely, total energy  $E/t$  is convex as a function of electron density  $n$ . In order to check this possibility, we show, in Fig. 8, the total energy of  $\Psi_Q^d$  and  $\Psi_Q^{\text{AF}}$  as a function of  $\delta$ . For both  $U/t = 8$  and  $12$ ,  $E/t$  of

the  $d$ -wave state exhibits a concave curve, namely  $\kappa > 0$ , meaning the  $d$ -wave state has intrinsic stability. In contrast, the AF state exhibits a convex curve,  $\kappa < 0$ , indicating that the AF state of partial filling gives rise to a phase separation of the insulating AF state with local filling  $\delta = 0$  and a SC (or normal) state with local filling  $\delta \gtrsim 0.2$ , according to the Maxwell construction. A similar result was reached by a recent QMC study for  $t' = 0$ .<sup>107)</sup> This instability does not occur in electron-doped cases as will be discussed for  $t' \neq 0$  in § 4.1, and in coexisting states of SC and AF.<sup>67,70)</sup>

### 3.3 $U/t$ dependence of correlation functions

To measure the strength of SC, a  $d_{x^2-y^2}$ -wave pairing correlation function,

$$P_d(\mathbf{r}) = \frac{1}{N_s} \sum_i \sum_{\tau, \tau' = \hat{x}, \hat{y}} (-1)^{1-\delta(\tau, \tau')} \times \langle \Delta_\tau^\dagger(\mathbf{R}_i) \Delta_{\tau'}(\mathbf{R}_i + \mathbf{r}) \rangle, \quad (20)$$

is appropriate for the present method. Here,  $\hat{x}$  and  $\hat{y}$  denote the lattice vectors in the  $x$  and  $y$  directions, respectively,  $\delta(\tau, \tau')$  indicates Kronecker delta, and  $\Delta_\tau^\dagger(\mathbf{R}_i)$  is the creation operator of a NN singlet pair at the site  $\mathbf{R}_i$ ,

$$\Delta_\tau^\dagger(\mathbf{R}_i) = (c_{i\uparrow}^\dagger c_{i+\tau\downarrow}^\dagger + c_{i+\tau\uparrow}^\dagger c_{i\downarrow}^\dagger) / \sqrt{2}. \quad (21)$$

If the value of  $P_d(\mathbf{r})$  remains finite for  $|\mathbf{r}| \rightarrow \infty$ , a  $d$ -wave off-diagonal long-range order exists. As explained in Appendix C, we found a proper scheme to reliably estimate  $P_d(\mathbf{r})$  for  $|\mathbf{r}| \rightarrow \infty$  ( $P_d^\infty$ ) from the data of finite  $L$ 's. We confirmed that  $P_d^\infty$  converges to zero for  $\Psi_Q^{\text{F}}$  and  $\Psi_Q^{\text{AF}}$  as  $L$  increases. Henceforth, we discuss  $P_d^\infty$ .

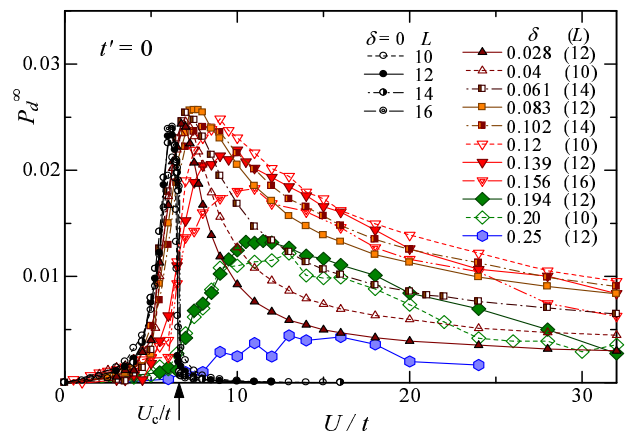


**Fig. 9.** (Color online)  $d$ -wave SC correlation function as function of  $U/t$  computed with  $d$ -wave states for various values of doping rate. Circle symbols indicate half filling ( $\delta = 0$ ); similarly, upward triangles ( $\Delta$ )  $\delta \sim 0.03$ , squares ( $\square$ )  $\delta \sim 0.09$ , downward triangles ( $\nabla$ )  $\delta \sim 0.14$ , diamonds  $\delta \sim 0.20$ , and hexagons  $\delta = 0.25$ . The arrow indicates the Mott critical value at half filling.

Figure 9 shows  $U/t$  dependence of  $P_d^\infty$  calculated with the optimized  $\Psi_Q^d$  for some  $\delta$ 's. Overall features for doped cases ( $\delta > 0$ ) resemble those of  $\Delta E/t$  (Fig. 3), especially for the optimal and overdoped regimes ( $\delta \gtrsim 0.15$ ). A large difference between  $P_d^\infty$  and  $\Delta E/t$  emerges as  $\delta$  approach

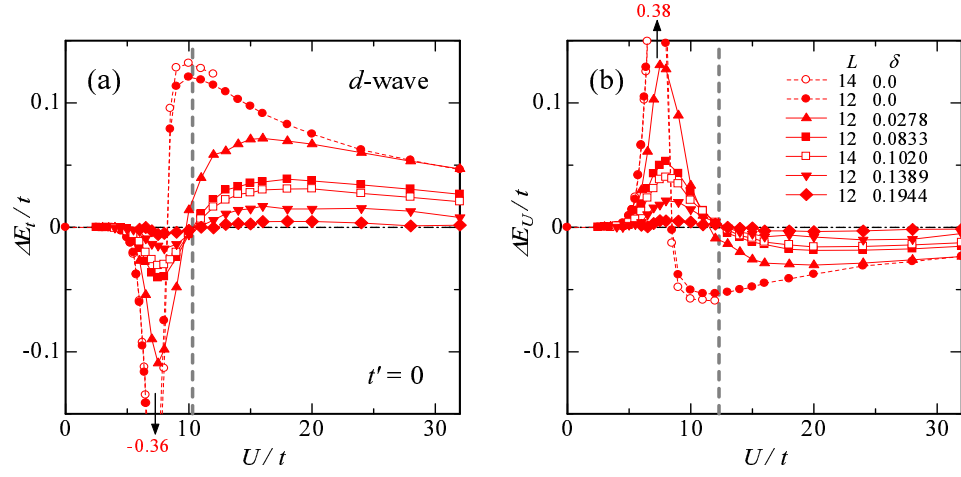


**Fig. 6.** (Color online) Components [(a) kinetic and (b) interaction parts] of energy gain  $\Delta E^d$  as function of  $U/t$ . The broad gray dashed lines roughly indicate the points where the signs of  $\Delta E_t$  and  $\Delta E_U$  are reversed.

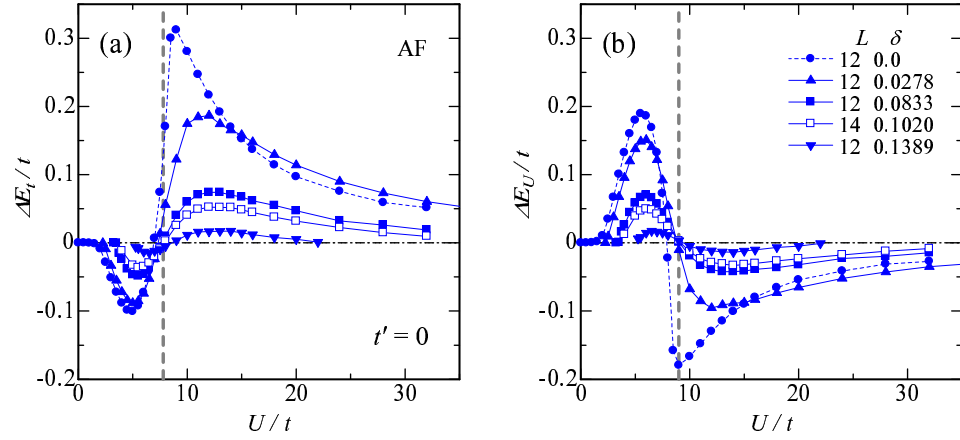


**Fig. 7.** (Color online) Components [(a) kinetic and (b) interaction parts] of energy gain  $\Delta E^{\text{AF}}$  as function of  $U/t$ . The broad gray dashed lines shows the same with those in Fig. 6.

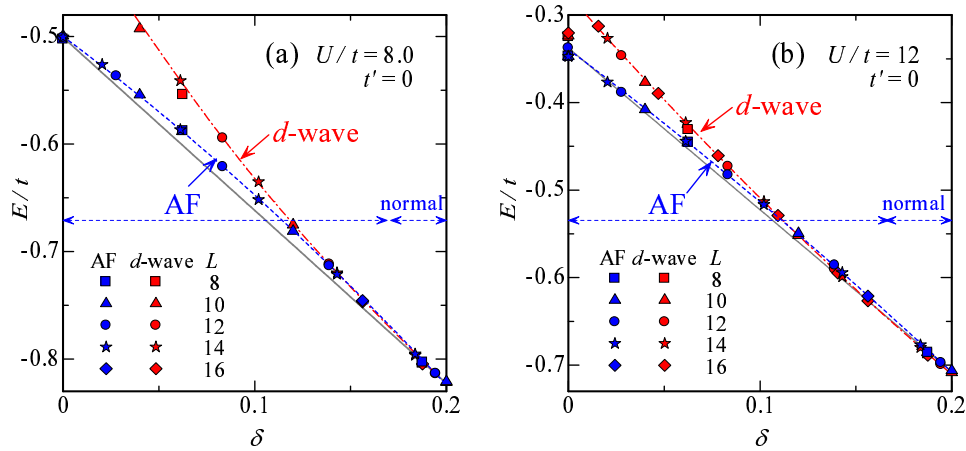


**Fig. 8.** (Color online) Total energy as function of doping  $\delta$  of AF and  $d$ -wave states for (a)  $U/t = 8$  and (b)  $U/t = 12$ . The AF state is reduced to a normal state for  $\delta \gtrsim 0.18$ , as shown with horizontal dashed arrows. The solid lines are straight guide lines.

rapidly as  $U/t$  increases. The extreme case is half filling, at which  $P_d^\infty$  vanishes for  $U > U_c$ , corresponding to the Mott transition, as discussed in ref. 17. Thus, the peak value of  $P_d^\infty$ , which is a better definition of  $U_{co}/t$ , decreases to the Mott critical value  $U_c/t$  as  $\delta$  decreases

We leave an analysis of the  $\delta$  dependence to the next subsection.



For SC in the present case, the spin structure factor,

$$S(\mathbf{q}) = \frac{1}{N_s} \sum_{ij} e^{i\mathbf{q} \cdot (\mathbf{R}_i - \mathbf{R}_j)} \langle S_i^z S_j^z \rangle, \quad (22)$$

is an important quantity, because the electron pair scattering with  $\mathbf{Q} = (\pi, \pi)$  will contribute to the  $d_{x^2-y^2}$ -wave pairing. In Fig. 10(a),  $U/t$  dependence of  $S(\mathbf{Q})$  calculated with  $\Psi_Q^d$  is plotted for six values of  $\delta$ . As discussed in ref. 17,  $S(\mathbf{Q})$  increases with  $U/t$ , and in particular, discontinuously at  $U_c/t$  at half filling in accordance with the first-order Mott transition. For  $\delta > 0$ ,  $S(\mathbf{Q})$  still rapidly increases for  $U_c \lesssim U \lesssim U_{co}$ , although the discontinuity vanishes. The increase of  $S(\mathbf{Q})$  for  $U < U_{co}$  coincides with the behavior of  $P_d^\infty$ , but the further increase of  $S(\mathbf{Q})$  for  $U > U_{co}$  is opposed to the decrease of  $P_d^\infty$ . This is because SC also depends on the itinerancy of carriers; for example, the quasiparticle renormalization factor  $Z$  in the nodal direction decreases as  $U/t$  increases [Fig. 6 in ref. 16].

Similar decreasing behavior is found in the charge correlation function between NN sites,

$$N_1 = \left| \frac{1}{4N_s} \sum_{j,\tau} \langle n_j n_{j+\tau} \rangle - n^2 \right|, \quad (23)$$

as shown in Fig. 10(b). Here,  $\tau$  runs over the four NN sites of the site  $j$ .  $N_1$  represents NN charge fluctuation, and is related to the mobility of electrons. The decrease of  $N_1$  and  $Z$ , showing suppression of charge fluctuation by  $U/t$ , resembles the behavior of  $P_d^\infty$  for  $U > U_c$ .

The above argument implies that the strength of SC requires two factors, namely, the pair formation owing to AF spin correlation and the fluidity of pairs owing to charge fluctuation. We argue this topic again in the light of  $\delta$  dependence, which is controllable in experiments of the cuprates, in the next subsection.

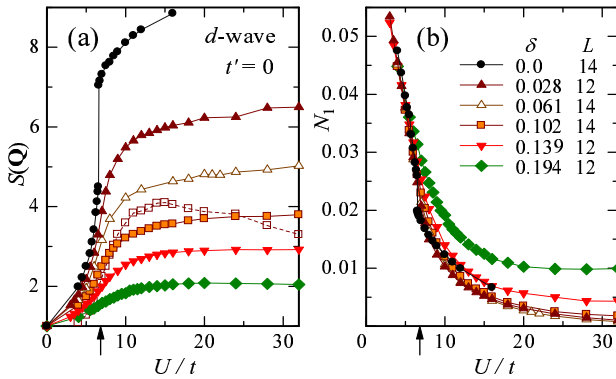


**Fig. 10.** (Color online) (a) Spin structure factor  $S(\mathbf{q})$  at  $\mathbf{q} = (\pi, \pi)$  for six electron densities. For comparison, the behavior of optimized  $d$ -wave gap parameter  $\Delta_d/t$  (exactly  $8\Delta_d/t + 1$ ) is also shown for  $\delta = 0.102$  (open square and dashed line). (b) Nearest-neighbor charge correlation function as function of  $U/t$ . The symbols for  $\delta$  and  $L$  are common between the two panels. The arrows indicate the Mott transition point at half filling.

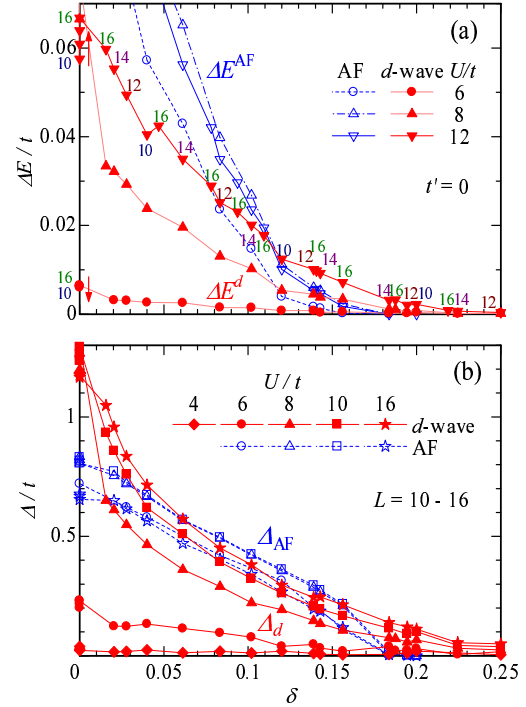


**Fig. 11.** (Color online) (a) Energy gain  $\Delta E/t$  for  $d$ -wave and AF states versus doping rate. The numbers near the data points indicate the used system sizes ( $L$ ). The arrows alongside the vertical axis denote the direction of system-size dependence at  $\delta = 0$  (downward:  $U/t = 6$ ; upward:  $U/t = 8$  and  $12$ ). (b) Optimized gap parameters in  $d$ -wave ( $\Delta_d$ ) and AF ( $\Delta_{AF}$ ) states as functions of doping rate.

### 3.4 Doping-rate dependence of various quantities

First, we look at the energy gain of the  $d$ -wave state  $\Delta E^d$  [eq. (17)]. In Fig. 11(a), we show the  $\delta$  dependence of  $\Delta E^d$ ;  $\Delta E^d$  is the largest at half filling and monotonically decreases as  $\delta$  increases for any  $U/t$ . Figure 11(b) shows the  $\delta$  dependence of optimized  $d$ -wave gap  $\Delta_d$ , which is the sole parameter directly controlling the energy scale of a singlet gap in  $\Psi_Q^d$ . It is natural to consider that  $\Delta_d$  corresponds to the pseudogap.<sup>92,108</sup>  $\Delta_d$  is highly similar to that of  $\Delta E^d$  as in the  $U/t$  dependence. Thus, we find again that  $\Psi_Q^d$  is stabilized by the  $d$ -wave singlet formation. We will see the relation of these quantities to the spin correlation shortly.

Next, we consider the  $d$ -wave SC correlation  $P_d^\infty$ ; its  $\delta$  dependence is shown in Fig. 12. For  $U/t = 4$ , the magnitude of  $P_d^\infty$  is very small and has relatively large  $L$  and  $\delta$  dependence, indicating that firm SC is unlikely to appear for  $U/t = 4$ . This result is consistent with those of QMC calculations,<sup>8,9,61</sup> in which the increase in SC correlations as  $U/t$  increases is not found for small  $U/t$ 's. When  $U/t$  is just below the Mott transition point  $U_c/t$  ( $\sim 7$ ), as in  $U/t = 6$ ,  $P_d^\infty$  has the maximum at half filling, and is basically a decreasing function of  $\delta$ , except for the fluctuation in  $L$  (and  $\delta$ ). This large system-size dependence suggests that the SC is still fragile. These results for  $U < U_c$  indicates that  $T_c$  does not exhibit a dome shape in the weakly correlated Hubbard model, although the approximate methods claim such behavior.<sup>6,109</sup>

In contrast,  $P_d^\infty$  for  $U > U_c$  displays a dome shape

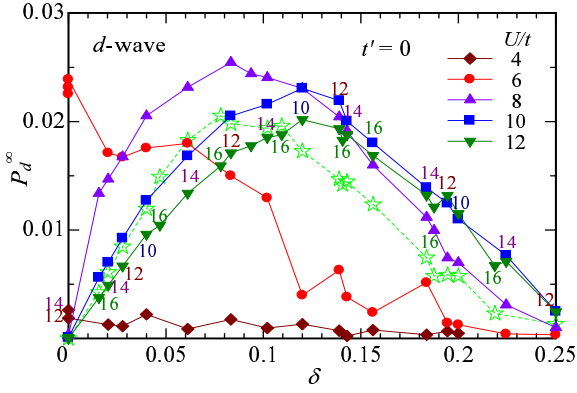


**Fig. 12.** (Color online)  $d$ -wave SC correlation function versus doping rate for several values of  $U/t$  in  $\Psi_Q^d$ . The digits (10-16) denote the system size  $L$  used. The stars denote  $\Delta_{SC}^2$  for  $U/t = 12$  calculated with eq. (24) using  $\Delta_d$  obtained by VMC. The magnitude of  $\Delta_{SC}^2$  is adjusted to be equal with the corresponding  $P_d^\infty$ .

as a function of  $\delta$ , which is caused by the vanishing of  $P_d^\infty$  at half filling as a Mott insulator. The shape of  $P_d^\infty$ , especially for  $U/t = 12$ , closely resembles that of the SC order parameter for the NN pairing  $|\langle c_{0\uparrow}^\dagger c_{\tau\downarrow}^\dagger \rangle|$  obtained in the  $t$ - $J$  model,<sup>13)</sup> and is consistent with the experimental results of  $T_c$  and condensation energy in cuprates. For these  $U/t$ 's, SC is considered robust owing to the small system-size dependence. This result claims that the effective correlation strength in cuprates be strong, i.e.,  $U > U_c$ . Thus, the high- $T_c$  cuprates are literal “doped Mott insulators”.<sup>1, 4, 5)</sup>

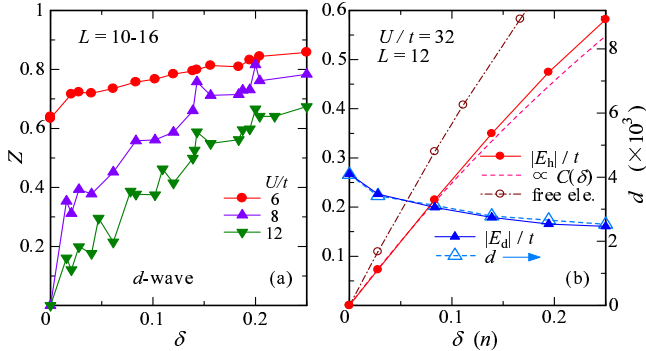


**Fig. 13.** (Color online) (a) Quasiparticle renormalization factor in nodal direction versus doping rate for  $d$ -wave state. (b) Absolute values of  $E_d$  and  $E_h$  are shown as functions of  $\delta$  by solid symbols in a strongly correlated case ( $U/t = 32$ ). For comparison, we add the doublon density (open triangle, right axis), a guide line  $\propto C(\delta) = 2\delta/(1+\delta)$  (dashed line), and the energy of free electrons as a function of electron density  $n$  (open circle).

For  $U > U_c$ ,  $P_d^\infty$  increases almost linearly to  $\delta$  in the underdoped regime, in contrast with the quantities like  $\Delta_d/t$  and  $\Delta E^d/t$ , which are monotonically decreasing functions of  $\delta$ . As mentioned, this is because the strength of SC depends on two factors, singlet-pair formation ( $\Delta_d$ ) and quantities related to charge transport like carrier density and mobility of carriers. The latter quantities are bound to increase as  $\delta$  increases for  $U > U_c$ , released from the vanishing of the correlation function in Mott insulators.

As an example, in Fig. 13(a), we show the quasiparticle renormalization factor  $Z$  estimated from the jumps in  $n(\mathbf{k})$  in the nodal direction. Since  $Z$  roughly represents the inverse effective mass,  $Z$  is zero at half filling and monotonically increases as  $\delta$  increases for  $U > U_c$ , in accordance with the result for the  $t$ - $J$  model.<sup>108)</sup>  $N_1$  [eq. (23)] and the conductive part of  $E_t$  discussed in §3.5 [ $|E_h|$  in Fig. 13(b)] are also increasing functions of  $\delta$ .

To consider  $\delta$  dependence of SC strength, it is useful to mention a simple analytic calculation. In a pioneering study using a Gutzwiller-type approximation for the  $t$ - $J$  model,<sup>92)</sup> a relation

$$\Delta_{SC} = \frac{2\delta}{1+\delta} \Delta_d. \quad (24)$$

was derived; here the energy scale of SC ( $\Delta_{SC}$ ) originates solely in  $\Delta_d$  ( $d$ -wave singlet gap), but modified by the factor of carrier density. As an example, we estimate  $\Delta_{SC}^2$  for  $U/t = 12$  using  $\Delta_d$  calculated by VMC, and the result is plotted in Fig. 12 by open stars.  $\Delta_{SC}^2$  qualitatively agrees with  $P_d^\infty$  for  $U/t = 12$ . A similar dome shape is also obtained from  $Z\Delta_d$ , instead of eq. (24). Note that in a slave-boson-mean-field theory,<sup>4, 110)</sup>  $T_c$  in the underdoped regime is determined by the Bose-condensation temperature  $T_B \propto \delta$  of holons, which represent the charge part of carriers.

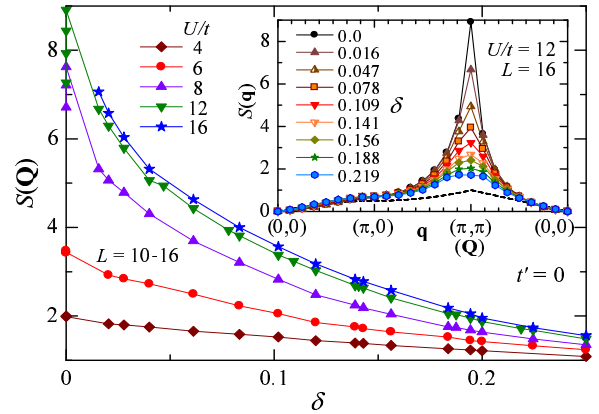


**Fig. 14.** (Color online) Spin structure factor at  $\mathbf{q} = (\pi, \pi)$  in  $d$ -wave state as function of doping rate for five  $U/t$ 's. The inset represents  $S(\mathbf{q})$  at  $U/t = 12$  for various doping rates along the path  $(0,0) \rightarrow (\pi,0) \rightarrow (\pi,\pi) \rightarrow (0,0)$ . The dashed line shows the value for  $U = 0$  and  $\delta = 0$ .

We turn to the spin structure factor  $S(\mathbf{q})$ . In the inset of Fig. 14,  $S(\mathbf{q})$  of  $\Psi_Q^d$  at  $U/t = 12$  is depicted for various  $\delta$ 's. A sharp peak at  $\mathbf{q} = \mathbf{Q}$  near half filling confirms a predominant AF spin correlation, and  $S(\mathbf{q})$  preserves the maximum at  $\mathbf{Q}$  for  $\delta \lesssim 0.2$ . The main panel of Fig. 14 shows the  $\delta$  dependence of  $S(\mathbf{Q})$  for five values of  $U/t$ ;  $S(\mathbf{Q})$  is a decreasing function of  $\delta$  for any correlation strength. The small system size dependence indicates a short-ranged nature of  $S(\mathbf{Q})$ . We here repeat the close connection between the spin correlation and the D-H binding correlation (Fig. 2);  $\delta$  dependences of  $\Delta E^d$ ,  $\Delta_d$  and  $S(\mathbf{Q})$  closely resemble to one another. This suggests a strong correlation between  $\Delta_d$  and AF spin correlation, namely, the energy of  $\Psi_Q^d$  is probably lowered

by the formation of  $d$ -wave singlet pairs through the AF spin correlation.

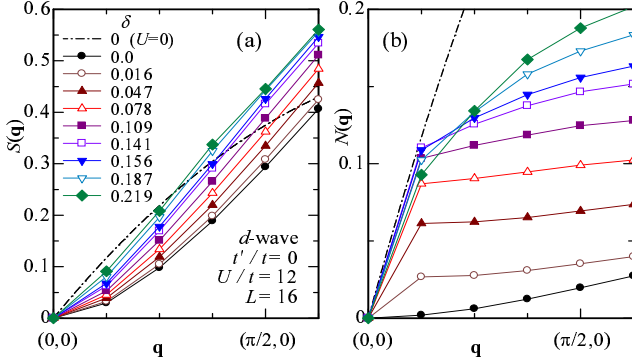


**Fig. 15.** (Color online) Small- $|\mathbf{q}|$  behavior of (a) spin and (b) charge density structure factors in  $(0,0)$ - $(\pi,0)$  direction for  $U/t = 12$  and some doping rates. In (b),  $N(|\mathbf{q}|) \propto |\mathbf{q}|^\gamma$  with  $\gamma \leq 1$  for  $\mathbf{q} \rightarrow 0$  seems to hold for  $\delta > 0$ . The system used and symbols of  $\delta$  are common to the two panels.

Now, we touch on how spin and charge density gaps evolve when  $\delta$  is introduced. It was revealed in ref. 17 for half filling that  $\Psi_Q^d$  has a finite spin (SC) gap for any positive  $U/t$ , but is gapless for  $U < U_c$  and gapped for  $U > U_c$  in the charge sector. It is known within the single-mode approximation<sup>111</sup> that a charge density gap opens [closes] if the charge density structure factor,

$$N(\mathbf{q}) = \frac{1}{N_s} \sum_{i,j} e^{i\mathbf{q} \cdot (\mathbf{R}_i - \mathbf{R}_j)} \langle n_i n_j \rangle - n^2, \quad (25)$$

behaves as  $N(\mathbf{q}) \propto |\mathbf{q}|^2$  [ $\propto |\mathbf{q}|$ ] for  $|\mathbf{q}| \rightarrow 0$ . For the spin sector, a similar treatment with  $S(\mathbf{q})$  is available. In Fig. 15, we show small- $|\mathbf{q}|$  behaviors of  $S(\mathbf{q})$  and  $N(\mathbf{q})$  at  $U = 12t$  ( $> U_c$ ) for various doping rates. A SC (singlet) gap survives up to the overdoped regime ( $\delta > 0.15$ ), although the quadratic feature of  $S(\mathbf{q})$  becomes less distinctive as  $\delta$  increases. On the other hand, in  $N(\mathbf{q})$ , the quadratic behavior immediately disappears on being doped, namely, the charge density gap vanishes for  $\delta > 0$ , because  $|\mathbf{q}|^2/N(\mathbf{q})$  seems to vanish for  $|\mathbf{q}| \rightarrow 0$ .

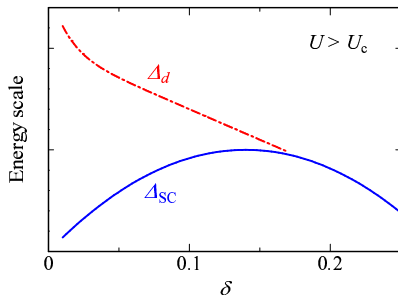


**Fig. 16.** (Color online) Schematic  $\delta$  dependence of two kinds of gap scales deduced from present calculations for  $U > U_c$ .

present calculations (Fig. 16). The gap scales representing the features of SC for  $U > U_c$  are classified into two kinds: (i) Quantities exclusively related to the singlet formation, which is derived from the superexchange interaction, monotonically decrease by doping, which weakens the AF correlation. They are symbolically indicated by  $\Delta_d$  in Fig. 16. (ii) Quantities directly related to SC, which is affected by both the singlet gap  $\Delta_d$  and charge transportability, increase as  $\delta$  increases in the underdoped regime, as shown by  $\Delta_{SC}$ . It is natural to substitute  $T_c$  ( $T_{\text{pair}}$ ) for  $\Delta_{SC}$  ( $\Delta_d$ ) in Fig. 16.

Finally, we touch on the relation between  $\Delta E^d$  in eq. (17) and the SC condensation energy experimentally observed ( $\Delta E_{\text{cond}}$ ). In the BCS theory,  $\Delta E^d$  coincides with  $\Delta E_{\text{cond}}$  at  $T = 0$ . However, this feature is not applicable to the present case, because only a part of  $\Delta_d$  contributes to  $\Delta_{SC}$  and the residual part remains as an incoherent singlet gap. Actually,  $\Delta E_{\text{cond}}$ 's estimated from the specific heat measurement<sup>112,113</sup> exhibit a dome shape as a function of  $\delta$  as in  $T_c$ , and is utterly different from the monotonic behavior of  $\Delta E^d$  shown in Fig. 11(b). Correctly, the above incoherent part should be cancelled with the corresponding part of a proper normal state; improvement of the normal state is necessary. Anyway, we should be prudent in comparing  $\Delta E^d$  with  $\Delta E_{\text{cond}}$ .

### 3.5 Mechanism of conduction

Here, we show that the mechanism of conduction undergoes a marked change through the crossover. To this end, it is useful to analyze the kinetic energy  $E_t$  into two components,  $E_t = E_d + E_h$ , according as the hopping process varies ( $E_d$ ) or does not vary ( $E_h$ ) the number of doublons,<sup>114</sup> as shown in Fig. 17(a).  $E_d$  is derived from the hopping processes of creating and destroying D-H pairs, and corresponds to the  $J$  term in the  $t$ - $J$  model.  $E_h$  comes from the direct hopping of holons and doublons, which corresponds to the  $t$  term in the  $t$ - $J$  model.<sup>115</sup> In Fig. 17(b), we plot  $E_d$  and  $E_h$  as a function of  $U/t$  for several  $\delta$ 's. The behavior of the two components changes definitely at approximately  $U_{co}/t$ .

We begin with the strongly correlated regime ( $U > U_{co}$ ). At half filling,  $E_h$  substantially vanishes in the Mott insulating regime ( $U > U_c$ );  $E_d$  remains finite and behaves proportionally to  $-4t^2/U$  ( $= -J$ ). Since the state is insulating,  $E_d$  here does not contribute to current, namely, local processes of creating and annihilating D-H pairs are only repeated. When carriers are doped, this behavior of  $E_d$  ( $\propto -J$ ) is basically unchanged; its magnitude decreases slowly as  $\delta$  increases, accurately corresponding to the decrease of doublon number, as shown in Fig. 13(b). Thus, the local D-H processes at  $\delta = 0$  remain intact for  $\delta > 0$ , meaning that  $E_d$  is not involved in conduction. On the other hand,  $E_h$  becomes finite and is still almost constant for  $U > U_{co}$  with the magnitude linear in  $\delta$  or  $\propto 2\delta/(1 + \delta)$  in eq. (24), as depicted in Fig. 13(b). This indicates that independent motion of doped holons is realized for  $U > U_{co}$ , although their mass is somewhat heavier than that of the free electrons. It follows that two kinds of holons play entirely different roles in SC: one is related to the D-H pairs, and the other is related to the independent motion of doped holons.

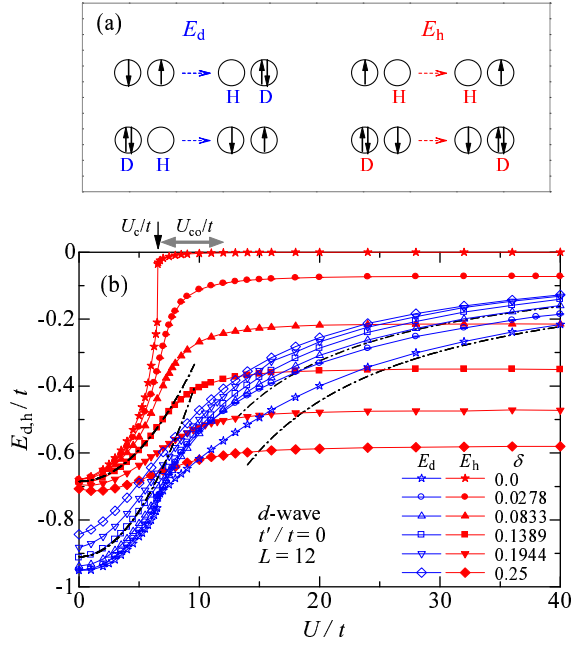


**Fig. 17.** (Color online) (a) Hopping processes which contribute to the two components of kinetic energy  $E_d$  and  $E_h$  are schematically shown. (b)  $U/t$  dependences of  $E_d$  and  $E_h$  are shown for six doping rates. The two dash-dotted lines in a small- $U/t$  [large- $U/t$ ] regime are guides as  $\sim (U/t)^2 + \text{const.}$  for  $\delta = 0.1389$  [ $\sim -t/U = -J/(4t)$  in  $E_d$  for  $\delta = 0$  and  $0.0833$ ].

devote themselves to forming local singlet pairs, whereas the holons introduced by doping work as current carriers, as schematically sketched in Fig. 18(b). Thus, the number of doped holes is equal to the number of carriers, which will make a small quasi Fermi surface like the Fermi arc or pocket. This feature is nothing but that of the  $t$ - $J$  model,<sup>5)</sup> and consistent with various experiments for the cuprates,<sup>116)</sup> and supports the very low superfluid densities.<sup>117)</sup> The residual (background) spinons (singly occupied sites) remain localized unless the doped holons collide with them; this fact is possibly related to a recent neutron scattering for Bi2212,<sup>118)</sup> which argued that the source of magnetic response in doped cuprates is localized spinons.

In contrast, for  $U < U_{co}$ , both  $E_d$  and  $E_h$  behave as

$$E_d \sim c_d U^2/t + E_d(0),$$

$$E_h \sim c_h U^2/t + E_h(0),$$

with  $c_d$  and  $c_h$  being constants, as shown in Fig. 17(b). This result indicates that every hopping process gives a contribution to  $E_t$  in the same way. Since the D-H binding is ineffective in this regime, holons cannot be classified into the two kinds, and all electrons contribute to conduction, as in Fig. 18(a), resulting in a large (ordinary) Fermi surface with the carrier number of  $N$ . Correspondingly, the number of doped holes discords with the carrier number, contrary to the experimental results in cuprates.

We have also obtained results similar to Fig. 17(b) for the normal and AF states, although we do not show here. The mechanism of conduction in doped Mott insulators entirely differs from that in weakly correlated systems.

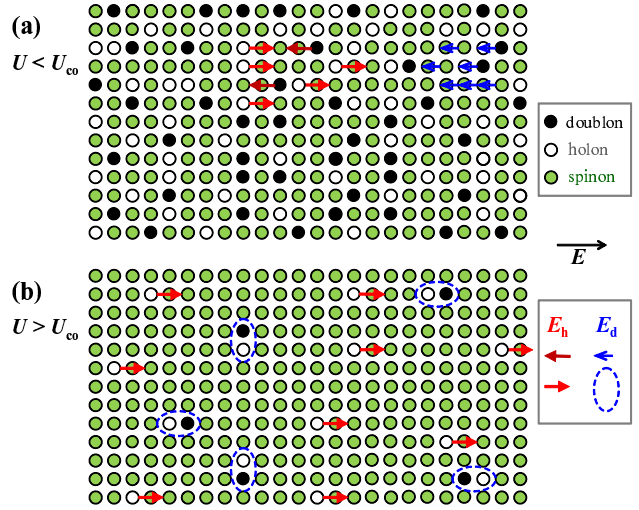


**Fig. 18.** (Color online) Mechanism of conduction is schematically compared between (a) the weakly correlated [Fermi liquid or BCS-type SC] regime and (b) the strongly correlated [doped Mott insulator] regime. Small arrows represent the motion of particles if a field ( $E$ ) is applied; in (a) arrows are drawn only for a small part of particles for clarity. The dashed ellipses in (b) indicate the local creation and annihilation processes of bound D-H pairs, which do not contribute to current.

#### 4. Effect of diagonal transfer $t'$

In this section, we study the effect of next-nearest-neighbor hopping ( $t'$ ), which is the principal term to characterize the individuality of each high- $T_c$  cuprate. In §4.1, we consider the stability of  $\Psi_Q^d$  against  $\Psi_Q^{AF}$  in introducing  $t'$  and possible phase separation near half filling. In §4.2, we discuss the origin of stability of  $d$ -wave and AF states on the basis of the effect of  $t'$ . In §4.3, we study the effect of  $t'/t$  on  $P_d^\infty$ , whereby we discuss the mechanism to enhance  $P_d^\infty$ .

##### 4.1 Energy gain by $d$ -wave gap

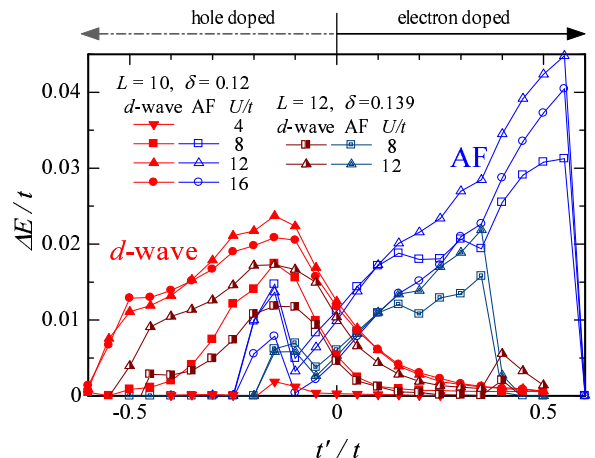


**Fig. 19.** (Color online) Energy gain for  $d$ -wave (solid and half-solid symbols) and AF (open and double-line symbols) states as function of  $t'/t$  for optimally-doped densities. For comparison, data for some values of  $U/t$  and two values of  $L$  are plotted.

At half filling, we now focus on the range  $t'/t < 0$ .



because there is a symmetry between  $t'$  and  $-t'$ , as discussed in ref. 17 and Appendix A. On doping carriers, however, this symmetry is broken. Figure 19 shows  $\Delta E^d$  and  $\Delta E^{\text{AF}}$  for some  $U/t$ 's as a function of  $t'/t$  at roughly optimally doped densities  $\delta = 0.12$  and  $0.139$ . For the hole-doped cases ( $t'/t < 0$ ),  $\Delta E^d$  tends to be enhanced, and  $\Delta E^{\text{AF}}$  is suppressed. For  $U/t \geq 8$ ,  $\Delta E^d$  has a broad maximum in the range  $-0.3 \lesssim t'/t \lesssim -0.1$ , and tends to vanish relatively rapidly for  $t'/t \lesssim -0.45$ . In contrast,  $\Delta E^{\text{AF}}$  vanishes except for a small peak at  $t'/t \sim -0.15$ . This peak is caused by the overlap of the Fermi surface with flat-band parts near  $(\pi, 0)$ , as we will discuss later for  $\Psi_Q^d$ . For the electron-doped cases ( $t'/t > 0$ ), the situation is opposite.  $\Delta E^d$  gradually and monotonically decreases as  $t'/t$  increases, whereas  $\Delta E^{\text{AF}}$  monotonically increases until sudden breakdown at a large  $t'/t$ .

The  $U/t$  dependences (not shown) of  $\Delta E^d$  and  $\Delta E^{\text{AF}}$  are qualitatively similar to those for  $t' = 0$  in Fig. 3, although the overall amplitude depends on  $t'/t$  as in Fig. 19.

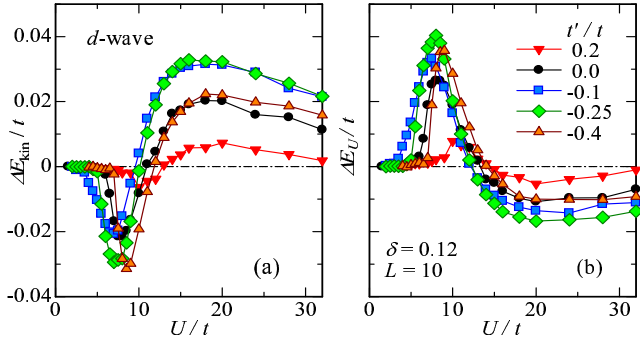


**Fig. 20.** (Color online) (a) Kinetic and (b) interaction parts of energy gain  $\Delta E^d$  for various values of  $t'/t$  as function of  $U/t$ .

We touch on the components of the energy gain  $\Delta E$  for finite  $t'/t$ . For small  $|t'/t|$ , the sum of  $\sigma_1(\omega)$  becomes approximately connected to the kinetic energy  $E_{\text{kin}}$ . In Figs. 20(a) and 20(b), we plot the kinetic ( $t$  and  $t'$  terms) and interaction parts of  $\Delta E$ , respectively, as functions of  $U/t$ . The behavior of the two components are qualitatively identical to that for  $t' = 0$  (Fig. 6): SC is induced by the reduction in interaction (kinetic) energy for small (large)  $U/t$ 's. Here, the doping rate is fixed at  $\delta = 0.12$ , but the tendency is unchanged for other  $\delta$ 's.

In §3.2, we showed that  $\Psi_Q^{\text{AF}}$  is unstable against phase separation for  $t' = 0$  (Fig. 8). Here, we discuss the tendency toward the phase separation for  $t' \neq 0$ . In Fig. 21, we plot the total energy of the AF and  $d$ -wave states as functions of  $\delta$  for hole- and electron-doped cases. For  $\Psi_Q^d$ ,  $E^d/t$  is concave ( $\kappa > 0$ ) for both values of  $t'/t$ , indicating that the  $d$ -wave state is still stable if  $t'$  is added, regardless of the kind of doped carriers. For the AF state, it becomes slightly concave for  $t'/t = 0.2$  (electron-doped case) [Figs. 21(b)], indicating that the commensurate AF state is intrinsically stable for the electron doping. On the other hand,  $E^{\text{AF}}/t$  is still convex ( $\kappa < 0$ ) for  $t'/t = -0.10$  (hole-doped cases) in the whole range of finite optimized  $U/t$  ( $0 < U/t \leq 3.15$ ) [Fig. 21(a)]. This is a subtle but

a phase separation occurs in the underdoped regime as in  $t' = 0$ . Such behavior is almost independent of the value of  $U/t$  as far as  $U/t$  is sufficiently large; the same behavior has been found for the  $t$ - $J$  model.<sup>119)</sup>

The reason of this instability of the AF state seems trivial; doping rapidly deteriorates the nesting of the Fermi surface for  $t'/t < 0$ , in contrast with the case of  $t'/t > 0$ . Although we have to be careful to compare directly the present result with experiments, because the band renormalization effect is not explicitly introduced in  $\Psi_Q^d$  and  $\Psi_Q^{\text{AF}}$ , there are some suggestive experiments: A neutron scattering experiment in very lightly doped  $\text{La}_{2-x}\text{Sr}_x\text{CuO}_4$  with  $x < 0.02$ <sup>120)</sup> found a phase separation to a commensurate AF ordered phase and a spin-glass phase. On the other hand, such a phase separation does not appear in the electron doped  $\text{Pr}_{1-x}\text{LaCe}_x\text{CuO}_4$ .<sup>120, 121)</sup>

#### 4.2 Origin of $t'$ -dependence regarding stability of $d$ -wave and AF states

The  $t'/t$  dependence of  $\Delta E^d$  and  $\Delta E^{\text{AF}}$  in the optimally doped regime (Fig. 19) is basically unchanging if  $\delta$  varies, as shown in Fig. 22 for  $U/t = 12$ . For  $t'/t = 0.2$  (solid symbols), we have  $\Delta E^{\text{AF}} > \Delta E^d$  for any  $\delta$ ; for  $t'/t = 0$  (half solid symbols) and  $-0.1$  (double-line symbols),  $\Delta E^{\text{AF}}$  and  $\Delta E^d$  interchange at  $\delta \sim 0.89$  and  $0.91$ , respectively, whereas for  $t'/t = -0.25$  (open symbols), we always have  $\Delta E^{\text{AF}} < \Delta E^d$ . Thus, the range of  $\delta$  where  $\Psi_{\text{AF}}$  ( $\Psi_d$ ) is predominant rapidly shrinks as  $|t'/t|$  increases on the hole- (electron-)doped side. Incidentally, we find  $\Delta E^{\text{AF}}$  remains small near half filling for  $t'/t = 0.2$  and  $-0.25$ . This is probably because the renormalization of the Fermi surface is not explicitly introduced in  $\Psi_Q^{\text{AF}}$ ; this effect becomes serious for  $\delta \rightarrow 0$  to retrieve the nesting condition.<sup>122, 123)</sup> We expect  $\Delta E^{\text{AF}} > \Delta E^d$  for  $\delta \sim 0$  even for large  $|t'/t|$  in improved calculations.

On the basis of Figs. 19 and 22, let us think about the stability of  $d$ -wave and AF states with respect to  $t'/t$ . As  $|t'/t|$  increases, the curvature of the Fermi surface in  $\Phi_F$  becomes more concave in the nodal direction  $(0, 0)$ - $(\pi, \pi)$  as shown in the inset of Fig. 22. Furthermore, it is expected that the scattering with  $\mathbf{q} = \mathbf{Q}$  is activated in the area of doped Mott insulators, as discussed in §3.3 and §3.4.

First, we discuss the origin of stability of  $\Psi_Q^{\text{AF}}$ . In the electron-doped cases, the nesting does not deteriorate rapidly when  $\delta$  increases away from half filling, namely, the Fermi surface continues to largely overlap with the magnetic Brillouin zone boundary as a whole, as shown in the inset of Fig. 22. The effect of large density of state near  $(\pi, 0)$  [see Fig. 23] is subsidiary for  $\Psi_Q^{\text{AF}}$ . On the other hand, the Néel order disappears rather suddenly, when  $t'/t$  becomes excessively large or holes are doped, because the nesting condition becomes insufficiently satisfied. Since the band renormalization effects becomes important for the AF order for  $U > W$ ,<sup>88, 123)</sup> we will reconsider it in future publications.

In contrast, conceivable reasons why the  $d$ -wave favors finite negative values of  $t'/t$  are as follows: (i) Because the

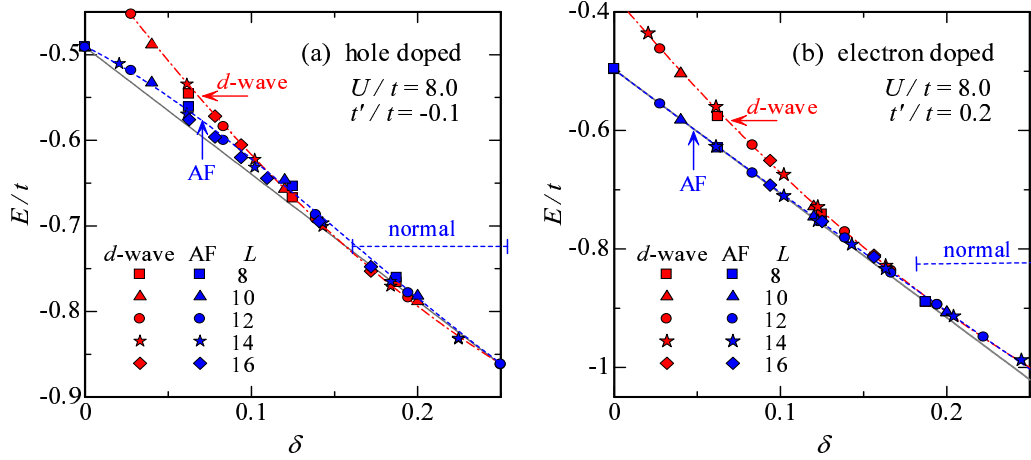


**Fig. 21.** (Color online) Total energy of  $d$ -wave ( $\Psi_Q^d$ ) and AF ( $\Psi_Q^{AF}$ ) states as function of doping rate. In (a) and (b), a hole-doped ( $t'/t < 0$ ) and an electron-doped ( $t'/t > 0$ ) cases are plotted, respectively. The data for several system sizes are fitted by the method of least squares, and shown with dashed (AF) and dash-dotted ( $d$ -wave) lines. The gray solid lines are straight guide lines for the AF case. In the region indicated by ‘normal’, the optimized AF state is reduced to the normal state, namely,  $\Delta_{AF} = 0$ . In (b), we omit the data of  $\Psi_Q^{AF}$  in the very vicinity of half filling owing to an abrupt phase change in  $\Psi_Q^{AF}$ . Similar data for  $t' = 0$  are given in Fig. 8.

$d$ -wave gap is minimum in the nodal directions and maximum in the antinodal ( $k_x$  and  $k_y$ ) directions, the energy gain is large when the electrons near  $(0, \pi)$  and  $(\pi, 0)$  are occupied. (ii)  $\mathbf{k}$ -dependent density of state,  $1/|\nabla\varepsilon(\mathbf{k})|$ , is minimum in the nodal direction including  $(\pi/2, \pi/2)$ , but becomes large near the antinodal points  $(\pi, 0)$  and  $(0, \pi)$  owing to the band flatness. Actually,  $1/|\nabla\varepsilon(\mathbf{k})|$  becomes large for  $t'/t = -0.3$  as  $\mathbf{q}$  approaches  $(\pi, 0)$  from  $(0, 0)$ , as in the dashed lines in Fig. 23, which shows  $1/|\nabla\varepsilon(\mathbf{k})|$  in the noninteracting case. (iii) The vector  $\mathbf{Q}$  connects two  $\mathbf{k}$  points near two nearest antinodal points with mutually inverse signs of  $\Delta_{\mathbf{k}}$ . Thus,  $\Psi_Q^d$  can take advantage

of  $d$ -wave pair scattering of  $\mathbf{Q}$  near the antinodal points, whereas the scattering around  $(\pi/2, \pi/2)$  seems of little importance. We will pursue this topic in §4.3 and §5.

This feature is corroborated by the behavior of the momentum distribution function,

$$n(\mathbf{k}) = \frac{1}{2} \sum_{\sigma} \langle c_{\mathbf{k}\sigma}^{\dagger} c_{\mathbf{k}\sigma} \rangle. \quad (26)$$

Figure 23 compares  $n(\mathbf{k})$  among the optimized  $d$ -wave, AF and normal states for an underdoped density.  $n(\mathbf{k})$  of the normal state exhibits clear discontinuities (Fermi surface) near  $(\pi, 0)$  and  $(\pi/2, \pi/2)$ . Near  $(\pi, 0)$ ,  $n(\mathbf{k})$ 's of both  $d$ -wave and AF states are considerably modified, meaning scattering actively takes place there. Near  $(\pi/2, \pi/2)$ ,  $n(\mathbf{k})$  of the AF state is again noticeably changed from that of the normal state depending on  $t'/t$ ,

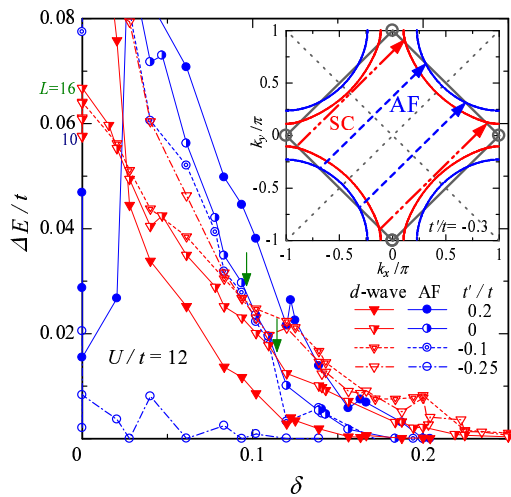


**Fig. 22.** (Color online) Comparison of energy gain between  $d$ -wave (triangles) and AF (circles) states as function of doping rate for four  $t'/t$ 's and  $U/t = 12$ . The arrows indicate the crossing points of  $\Delta E^{AF}$  and  $\Delta E^d$  for  $t'/t = 0$  and  $-0.1$ . Systems of  $L = 10$ -16 are used. The inset shows the Fermi surface in the electron picture for  $n = 0.85$  (favored by  $d$ -wave) and  $1.10$  (favored by AF) both for  $t'/t = -0.3$ . The arrows are the  $\mathbf{Q}$  vectors connecting the hot spots [intersections of the Fermi surface and magnetic Brillouin zone boundary indicated by the gray bold line]. The gray dotted lines indicate the nodes of the  $d$ -wave state, and the gray circles the van Hove singularity points near the Fermi surface.

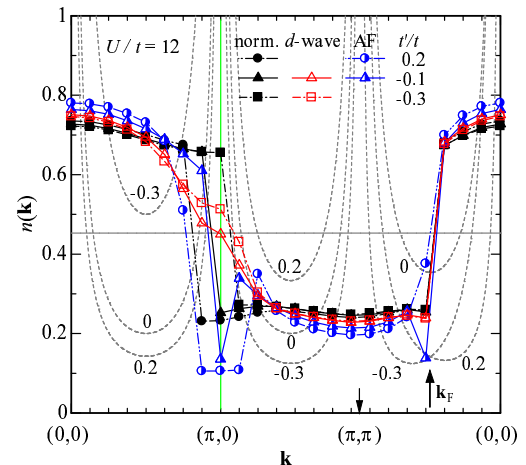


**Fig. 23.** (Color online) The momentum distribution functions are compared among the  $d$ -wave (open symbols), AF (half closed) and normal (closed) states for a couple of  $t'/t$ 's,  $\delta = 0.094$  and  $L = 16$ . Firm orders exist for the  $d$ -wave and AF states. The gray horizontal line shows  $n/2$ . The gray dashed curves represent the relative magnitude of noninteracting  $\mathbf{k}$ -dependent density of states



but  $n(\mathbf{k})$  of the  $d$ -wave state changes only slightly, and is almost independent of  $t'/t$ . Thus, for  $\Psi_Q^d$ , the scattering in the nodal direction is ineffective, but the electronic state near the antinodal points should be noticed.

#### 4.3 $d$ -wave pairing correlation

Now, we turn to the  $d$ -wave SC correlation function in  $\Psi_Q^d$ . In Fig. 24,  $U/t$  dependence of  $P_d^\infty$ , defined by eq. (20) and in Appendix C, is shown for four finite  $t'/t$ 's. In Fig. 25,  $\delta$  dependence of  $P_d^\infty$  is shown for four  $U/t$ 's. Although the overall behavior is similar to the case of  $t' = 0$  (Figs. 9 and 12), there are noteworthy differences owing to the effect of  $t'$ . (i) The magnitude of  $P_d^\infty$  is somewhat enhanced for  $t'/t = -0.1$  and  $-0.25$ , but is suppressed for  $t'/t = 0.2$ , in accordance with the behavior of  $\Delta E^d$  discussed in §4.1. (ii) For  $U > U_c$ , the doping rate giving the maximum  $P_d^\infty$  for a fixed value of  $U/t$  shifts to the overdoped side as  $t'/t$  decreases. (iii) For  $t'/t = -0.1$ ,  $P_d^\infty$  starts to increase at a smaller value of  $U/t$ . (iv) Although we do not show detailed data in Fig. 24, for  $t'/t \lesssim -0.4$  and  $\delta \gtrsim 0.2$ , a state with large  $P_d^\infty$  is competitive with a state with tiny  $P_d^\infty$  ( $\Delta_d/t \sim 0$ ), suggesting that the SC state collapses at approximately these parameters.

First, let us consider the point (i) and (ii) in the strongly correlated regime. As in Fig. 25(d), for  $U(=12t)$  sufficiently larger than  $U_c$ ,  $P_d^\infty$  forms a well-proportioned dome shape as a function of  $\delta$ . This  $\delta$  dependence of  $P_d^\infty$  is consistent with that of  $T_c$  and condensation energy observed in cuprates. We define  $\delta_{\max}$  as the value of  $\delta$  which marks the largest  $P_d^\infty$  for given  $U/t$  and  $t'/t$ . For  $\delta < \delta_{\max}$ ,  $P_d^\infty$  is proportional to  $\delta$ , and is almost independent of the values of  $t'/t$  and  $L$ . This means that SC in the underdoped regime is steady, and the magnitude of  $P_d^\infty$  depends only on  $U/t$ , and not on minute band structure. On the other hand, for  $\delta > \delta_{\max}$  for the hole-doped cases ( $t'/t < 0$ ),  $P_d^\infty$  irregularly depends on the values of  $t'/t$  and  $L$ , and is scattered to some extent.<sup>124)</sup> Thus, the strength of SC is sensitive to the shape of Fermi surface and fragile in the overdoped regime. However,  $P_d^\infty$  becomes larger than that for  $t' = 0$ , probably because the  $t'$  term bends the Fermi surface so that it may pass by the antinodal points. Similar behavior has been known for the  $t$ - $J$  model.<sup>51,88)</sup> For the electron-doped case,  $\delta_{\max}$  is smaller than those for the hole-doped cases, but the fluctuation with respect to  $\delta$  and  $L$  is small for  $\delta > \delta_{\max}$ , so that SC is steady. In the transitional regime [Fig. 25(c) for  $U_c < U \lesssim U_{co}$ ], although  $P_d^\infty$  manages to preserve the dome shape,  $\delta_{\max}$  is lowered to have a wide irregular range for  $t'/t < 0$ . For the electron-doped case ( $t'/t = 0.2$ ),  $P_d^\infty$  is suppressed as compared with  $t'/t = 0$ , and almost vanishes in the overdoped regime. Some similar features were pointed out in a recent study by Tocchio *et al.*<sup>125)</sup>

Next, we look at the case of intermediate correlation strength [ $U = 6t$ , Figs. 25(b)], which is slightly smaller than the Mott critical value  $U_c$ . As discussed in ref. 17,  $P_d^\infty$  for  $t' = 0$  exhibits a sharp peak immediately below  $U_c$  ( $\sim 7t$ ) at half filling; such behavior is unchanged for  $t' \neq 0$  (black circle symbols in Fig. 24). Because the value

largest at half filling, and tends to decrease as  $\delta$  increase. Especially for  $t'/t = -0.4$  and  $0.2$ ,  $P_d^\infty$  almost vanishes for  $\delta > 0.05$ . Similarly to the case of  $t' = 0$ , this behavior of  $P_d^\infty$  is contradictory to the dome shape of  $T_c$  and condensation energy observed in the cuprates, in contrast with the cases of  $U > U_c$ .

Now we move to the point (iii) regarding small values of  $U/t$ . As discussed in §3.3 for  $t' = 0$ ,  $P_d^\infty$  is negligibly small for  $U/t$  as small as 4. As found in Fig. 24, this feature basically does not alter even if  $t'$  is added, except for  $t'/t = -0.1$  [Fig. 24(a)]. This exceptional enhancement of  $P_d^\infty$  is evident in Fig. 25(a), where appreciable magnitude appears only for  $t'/t = -0.1$  in the six values of  $t'/t$ . We argue in the following that this exceptional enhancement of  $P_d^\infty$  at  $t'/t \sim -0.1$  for a small  $U/t$  is useful to infer the origin of SC.

In Fig. 26, we show  $P_d^\infty$  for  $U/t = 4$  with star symbols as a function of  $t'/t$  for four  $\delta$ 's. For an underdoped density,  $\delta = 0.0833$  [Fig. 26(b)], the meaningful magnitude of  $P_d^\infty$  is limited to a narrow range of  $-0.16 \lesssim t'/t \lesssim -0.075$ . Similarly it is also limited to the range of  $-0.275 \lesssim t'/t \lesssim -0.075$  for an overdoped density,  $\delta = 0.1944$  [Fig. 26(d)]. These results are consistent with that of a recent QMC study,<sup>61)</sup> which concluded that the SC susceptibility vanishes for  $t' = 0$  but remains finite for  $t'/t = -0.2$  for  $U/t \leq 5$  in the optimally doped regime. In Fig. 26, we simultaneously plot the momentum distribution function  $n(\mathbf{k})$  calculated with  $\Psi_Q^F$  and  $\Psi_Q^d$  at a couple of available  $\mathbf{k}$  points near the antinodal point  $\pi(1, 0)$ , i.e.,  $\mathbf{X} = \pi(1, \frac{1}{L})$  and  $\mathbf{X}' = \pi(1 - \frac{2}{L}, \frac{1}{L})$ . As  $t'/t$  is increased,  $n(\mathbf{X})$  or  $n(\mathbf{X}')$  of  $\Psi_Q^F$  discontinuously drops from near unity to near zero, when the Fermi surface passes through the  $\mathbf{X}$  or  $\mathbf{X}'$  point, as indicated by arrows on the upper axes. Note that in each panel, the positions of the peak and shoulders of  $P_d^\infty$  precisely coincide with those at which the Fermi surface overlaps with antinodal  $\mathbf{k}$  points. As in Fig. 23,  $(\pm\pi, 0)$  and  $(0, \pm\pi)$  are van Hove singularity points for  $|t'/t| \leq 0.5$ , and connected one another by the AF vectors  $\mathbf{Q} = (\pi, \pm\pi)$ ,  $(\pm\pi, \pi)$ . It follows that the pair scattering with  $\mathbf{Q}$  and SC thereby are enhanced at the values of  $t'/t$  indicated by the arrows. This SC mechanism is consistent with the  $d$ -wave BCS theory.<sup>126)</sup>

However, this mechanism for small  $U/t$ 's has difficulties in explaining features of the high- $T_c$  cuprates. First, the effective values of  $t'/t$  of the cuprates show a relatively wide range; single-layer La systems and double-layer Y and Bi systems have  $t'/t \sim -0.1$  and  $-0.3$ , respectively.<sup>46–50)</sup> However, the above SC mechanism sensitively depends on  $t'/t$  or the band structure, and SC correlation is enhanced only in the limited range. It is unlikely that robust SC occurs at  $t'/t = -0.3$  in the whole relevant range of  $\delta$ . Second, it is probable that the magnitude of  $P_d^\infty$  discussed above is, as a matter of fact, much weaker. As shown in Fig. 25(a),  $P_d^\infty$  has a large and relatively regular system-size dependence, and consequently seems to become negligible for  $L \rightarrow \infty$ .

For comparison, we make the same analysis for a strongly correlated case,  $U/t = 12$  (Fig. 27). In the underdoped regime [panels (a) and (b)],  $P_d^\infty$  has appreciable

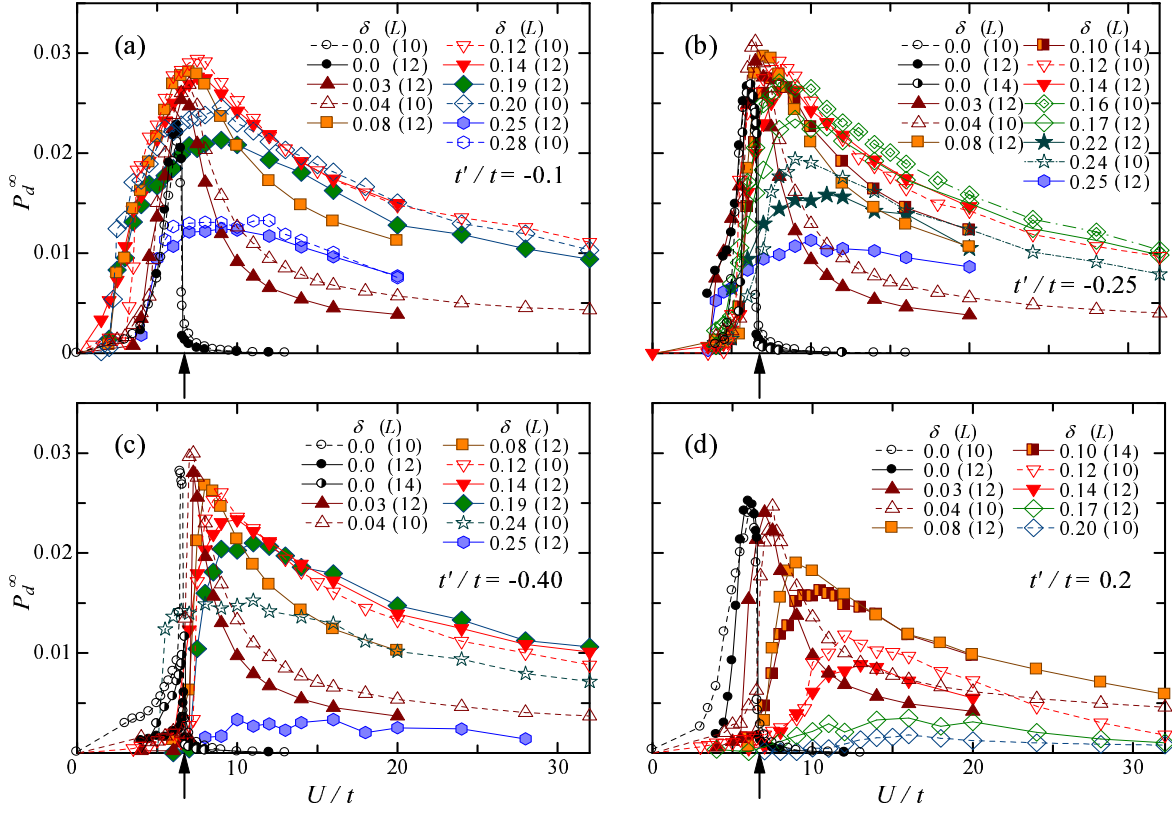


**Fig. 24.** (Color online)  $d$ -wave pairing correlation function as function of  $U/t$  for various values of doping rate  $\delta$  (rounded off to two decimal places in legends). The value of  $t'/t$  is different among the four panels: (a)-(c) hole-doped and (d) electron-doped cases. Corresponding results for  $t'/t = 0$  are given in Fig. 9. The arrow in each panel indicates the Mott transition point at half filling (circles).

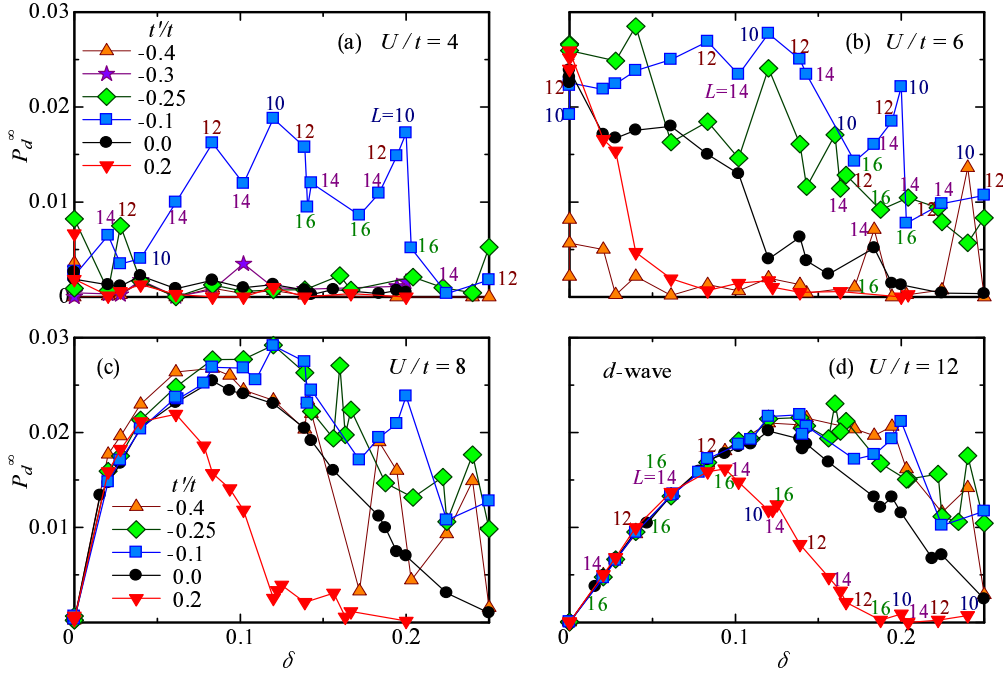


**Fig. 25.** (Color online)  $d$ -wave pairing correlation function as function of doping rate  $\delta$  for various values of  $t'/t$ . The value of  $U/t$  is different among the four panels (a)-(d). The symbols indicating the values of  $t'/t$  are common to the four panels. Small digits beside some data points indicate the used lattice size  $L$  ( $= 10-16$ ).

pendence is very weak, even between electron-doped and hole-doped cases [see also Fig. 28(c)]. In an optimum-

doping rate [Fig. 27(c)], the electron-hole asymmetry comes to stand out, and  $P_d^\infty$  decreases as  $t'/t$  increases

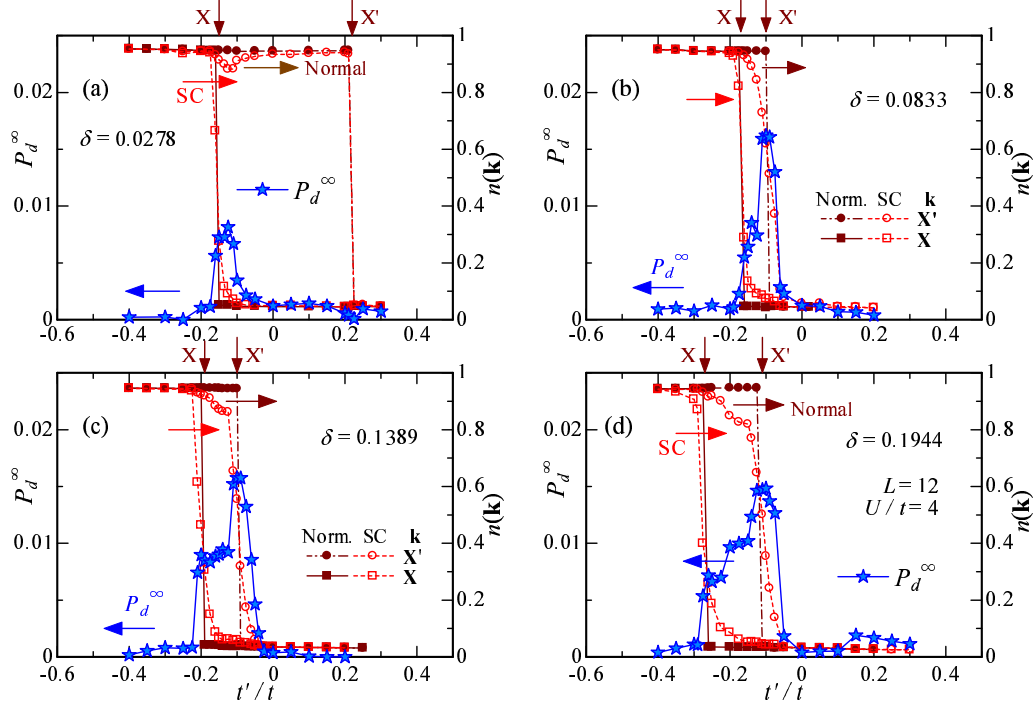


**Fig. 26.** (Color online) Correspondence between  $d$ -wave SC correlation function and jump in momentum distribution functions of  $\Psi_Q^F$  and  $\Psi_Q^d$  at two  $\mathbf{k}$  points ( $\mathbf{k} = \mathbf{X}$  and  $\mathbf{X}'$ ) near  $(\pi, 0)$ , as  $t'/t$  varies, for a weak correlation ( $U/t = 4$ ). The cases of four doping rates are shown for  $L = 12$ . The arrows on upper axes indicate the values of  $t'/t$  at which the Fermi surfaces of  $\Psi_Q^F$  pass  $\mathbf{X}$  and  $\mathbf{X}'$ .

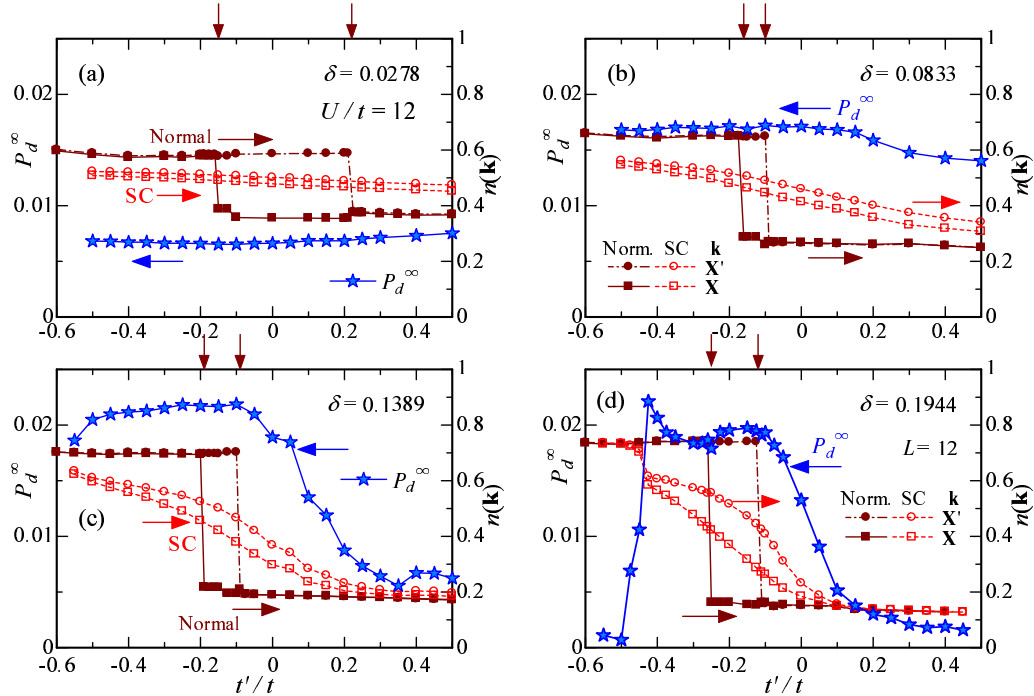


**Fig. 27.** (Color online) The same quantities as those in Fig. 26 are depicted in the same scales for a strongly correlation ( $U/t = 12$ ). The band renormalization by correlations is not considered here, but its effect seems irrelevant except near half filling.<sup>51, 88, 94, 123)</sup>

in the electron-doped regime  $t'/t > 0$ , but  $P_d^\infty$  is steady and large throughout the range of  $t'/t < 0$ . This tendency is preserved for an overdoped regime [Fig. 27(d)], where  $P_d^\infty$  is still large in the range of the hole-doped cuprates ( $-0.4 \lesssim t'/t \lesssim -0.05$ ). On the other hand, the Fermi surface of  $\Psi_Q^F$  passes  $\mathbf{k} = \mathbf{X}$  and  $\mathbf{X}'$  at the same  $t'/t$ 's as

the weakly correlated cases as indicated by arrows. For the underdoped and optimally-doped cases,  $P_d^\infty$  does not exhibit any special behavior at the positions of the arrows. Only in the overdoped case,  $P_d^\infty$  displays a slight tendency of forming a shoulder near an arrow. Anyway, in the strongly correlated regime, the strength of SC is al-

most independent of the locus of the Fermi surface of the underlying normal state, namely, the bare band structure, suggesting that  $P_d^\infty$  is determined by a mechanism qualitatively different from conventional BCS-type theories, which start from the instability of the Fermi surface of the normal state. We return to this subject in §5.

To summarize the  $t'/t$  dependence of  $P_d^\infty$ , we show  $P_d^\infty$  for three different regimes of  $\delta$  in Fig. 28. For a weak correlation ( $U/t = 4$ ), the area of enhanced  $P_d^\infty$  is limited ( $-0.25 \lesssim t'/t \lesssim -0.1$ ) regardless of  $\delta$ , and the magnitude tends to vanish as  $L$  increases. For strongly correlated cases ( $U/t \geq 8$ ),  $P_d^\infty$  is enhanced by moderate negative values of  $t'/t$ , when  $\delta$  is in the overdoped and optimally doped regime. On the other hand, near half filling, the magnitude of  $P_d^\infty$  is steady, and tends to be independent of  $t'/t$ , as  $U/t$  increases.

Finally, we point out that  $P_d^\infty$  becomes a weakly *increasing* function of  $t'/t$  near half filling and for very large  $U/t$ , as shown in Fig. 28(d). Such unexpected behavior was discovered for very slightly doped  $t$ - $J$  models, using density matrix renormalization group<sup>127)</sup> and exact diagonalization,<sup>128)</sup> and seemed incompatible with the property of cuprates. Afterward, a VMC study<sup>51)</sup> for the  $t$ - $J$  model revealed that this feature is restricted to the very vicinity of half filling. The present result supports this finding, and add a requirement that the interaction be considerably strong (e.g.  $U/t = 16$ ).

## 5. Antinodal Electrons and Superconductivity

In §4.2, we argued that the electrons near the antinodal points are crucial for the  $d$ -wave SC. In this section, we actually reveal a close relationship between the behavior of momentum distribution function  $n(\mathbf{k})$  near  $\mathbf{k} = (\pi, 0)$  and the SC correlation function  $P_d^\infty$  in the strongly correlated regime.

First, let us recall again the  $t'/t$  dependence of  $P_d^\infty$  for sufficiently large  $U/t$ 's to compare it with that of  $n(\mathbf{k})$ . As discussed in Ref. 17, properties of  $\Psi_Q^d$  in the insulating phase ( $U > U_c$  at half filling) are almost independent of  $t'/t$ . For small  $\delta$ , the  $t'/t$  dependence of  $P_d^\infty$  is still weak as seen for  $U/t = 12$  and 16 in Fig. 28(c), but for  $\delta \gtrsim 0.1$ ,  $P_d^\infty$  comes to largely depend on  $t'/t$ , i.e.,  $P_d^\infty$  tends to increase for  $t'/t < 0$  and decrease for  $t'/t > 0$  as in Figs. 28(b) and 28(a).

With this behavior of  $P_d^\infty$  in mind, we look at the  $t'/t$  dependence of  $n(\mathbf{k})$  [eq. (26)]. In Fig. 29,  $n(\mathbf{k})$  for six  $\delta$ 's is plotted for  $U/t = 12$ . In each panel, data for various values of  $t'/t$  are displayed together. At half filling [Fig. 29(a)],  $n(\mathbf{k})$  is almost independent of  $t'/t$  as mentioned, and does not have a discontinuity at any  $\mathbf{k}$ , because  $\Psi_Q^d$  is Mott insulating ( $U_c/t \sim 6.5$ -7.2) with a charge density gap. On doping carriers, a discontinuity (Fermi surface) appears in the lattice-diagonal direction near  $(\pi/2, \pi/2)$  [Figs. 29(b)- 29(f)],<sup>108)</sup> because  $\Psi_Q^d$  turns to SC with nodes of  $\Delta_{\mathbf{k}}$  for  $k_x = \pm k_y$  (and finally metallic). Meanwhile, it is in the antinodal area near  $(\pi, 0)$  where the behavior of  $n(\mathbf{k})$  markedly changes as  $t'/t$  varies; the degree of change culminates around the optimum doping rate ( $\delta \sim 0.15$ ). Compared with the antinodal area, the change in  $n(\mathbf{k})$  by  $t'/t$  is insignificant

close correspondence between SC correlation ( $P_d^\infty$ ) and the electronic structure in the antinodal area.

In the overdoped regime ( $\delta \gtrsim 0.2$ ),  $n(\mathbf{k})$  exhibits a Fermi-liquid-like discontinuity (Fermi surface) in the antinodal area for some  $t'/t$ 's, i.e., on the segment  $(0, 0)$ - $(\pi, 0)$  in the electron-doped cases ( $t'/t > 0$ ), and on  $(\pi, 0)$ - $(\pi, \pi)$  for  $t'/t \lesssim -0.4$  [Figs. 29(e) and 29(f)]. We find in Fig. 28(a) that when such a discontinuity appears, robust SC does not occur. Inversely, when  $n(\mathbf{k})$  changes continuously and relatively slowly in the antinodal area [Figs. 29(b)-(d)],  $P_d^\infty$  has a large and steady magnitude [Figs. 28(b) and (c)]. Such behavior appears in a broad range of  $t'/t$  particularly in the underdoped regime. We will discuss this problem shortly.

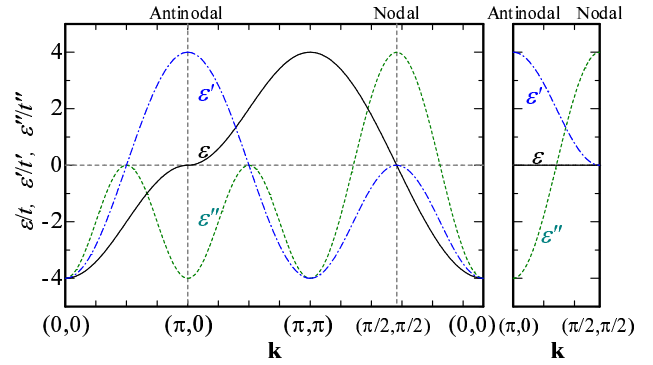


**Fig. 30.** (Color online) Elements of bare band dispersion relations along paths  $(0, 0) \rightarrow (\pi, 0) \rightarrow (\pi, \pi) \rightarrow (0, 0)$  (left panel) and  $(\pi, 0) \rightarrow (\pi/2, \pi/2)$  (right panel):  $\varepsilon/t = -2(\cos k_x + \cos k_y)$ ,  $\varepsilon'/t = -4 \cos k_x \cos k_y$ ,  $\varepsilon''/t = -2(\cos 2k_x + \cos 2k_y)$ .  $t''$  indicates the hopping integral to the third-neighbor sites  $(\pm 2, 0)$  and  $(0, \pm 2)$ , which is disregarded in this paper. The nodal  $(\pi/2, \pi/2)$  and antinodal  $(\pi, 0)$  points are marked by vertical dashed lines.

The above feature of  $n(\mathbf{k})$  is more or less related to the band structure. In Fig. 30, the elements of the bare band dispersion relation  $\varepsilon_{\mathbf{k}} [= \varepsilon + \varepsilon' (+\varepsilon'')]$  is depicted. The dispersion of the pure square lattice  $\varepsilon$  ( $t' = t'' = 0$ ) has a well-known flat part at  $\varepsilon = 0$  around  $(\pi, 0)$  (stationary in both  $k_x$  and  $k_y$  directions), where the Fermi surface passes for  $\delta \sim 0$ . The dispersion due to  $t'$  ( $\varepsilon'$ ) is also stationary but maximum at  $(\pi, 0)$ . Consequently,  $\varepsilon_{\mathbf{k}}$  and the locus of Fermi surface around  $(\pi, 0)$  sensitively depend on  $t'/t$ . In contrast, at the  $\varepsilon = 0$  point in the nodal direction  $(\pi/2, \pi/2)$ ,  $\varepsilon'$  is zero and stationary, so that the change of  $\varepsilon_{\mathbf{k}}$  by  $t'/t$  is slight near  $(\pi/2, \pi/2)$ . Incidentally, the third-neighbor hopping  $t''$ , which is omitted here but is often used as  $t'' = -t'/2$  in the literature, works similarly to that of  $t'$  near  $(\pi, 0)$  because  $\varepsilon''/t'' \sim -\varepsilon'/t'$ .<sup>129)</sup>

To relate the above feature of  $n(\mathbf{k})$  to  $P_d^\infty$  quantitatively, we need a quantity that appropriately expresses this feature. The magnitude of  $n(\mathbf{k})$  near  $(\pi, 0)$  itself apparently does not represent the strength of SC. In fact, we found that the slope of  $n(\mathbf{k})$ ,

$$|\nabla n(\mathbf{k})| = \sqrt{\left(\frac{\partial n(\mathbf{k})}{\partial k_x}\right)^2 + \left(\frac{\partial n(\mathbf{k})}{\partial k_y}\right)^2}, \quad (27)$$

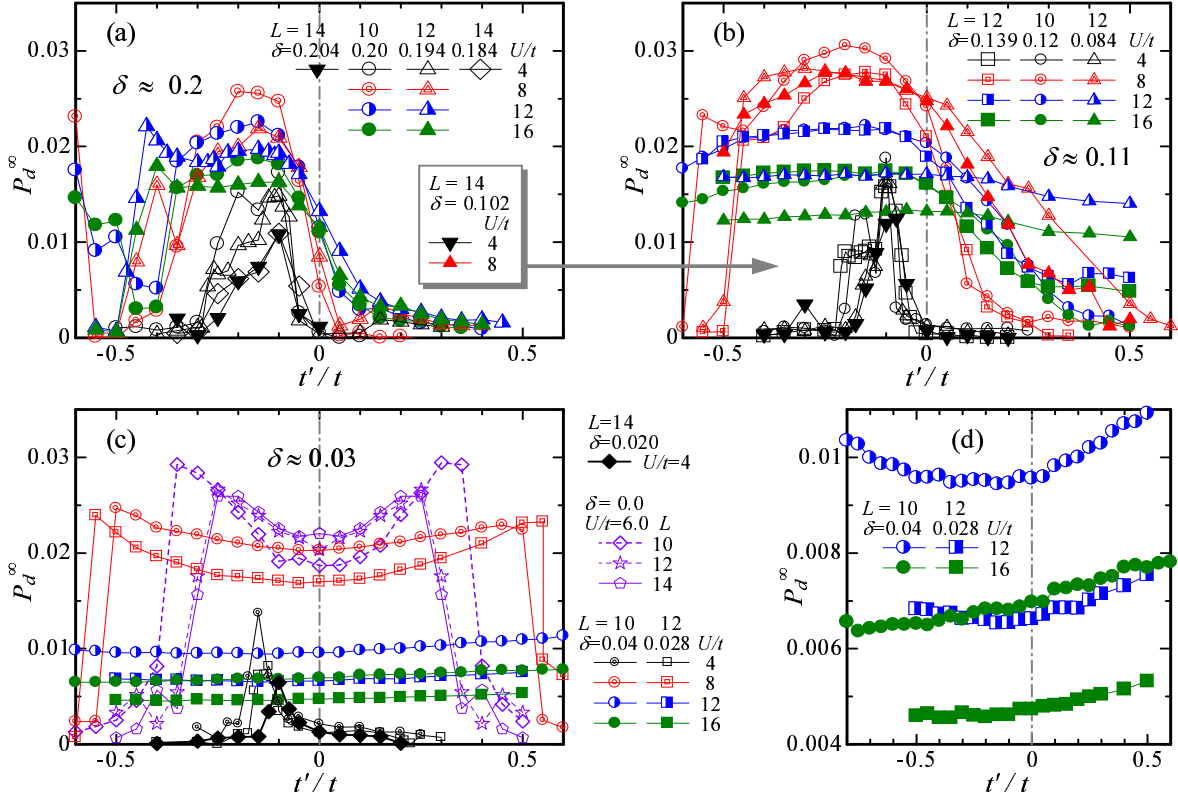


**Fig. 28.** (Color online)  $d$ -wave pairing correlation function as function of  $t'/t$  for several values of  $U/t$ . Doping rate  $\delta$  is different among (a)-(c): (a) in the overdoped regime,  $\delta \sim 0.20$ , (b) in the optimally doped and underdoped regime,  $\delta \sim 0.11$ , and (c) nearly half filling  $\delta \sim 0.03$ . In (d), a magnification of (c) in the vertical axis is shown to emphasize subtle variation of  $P_d^\infty$ .

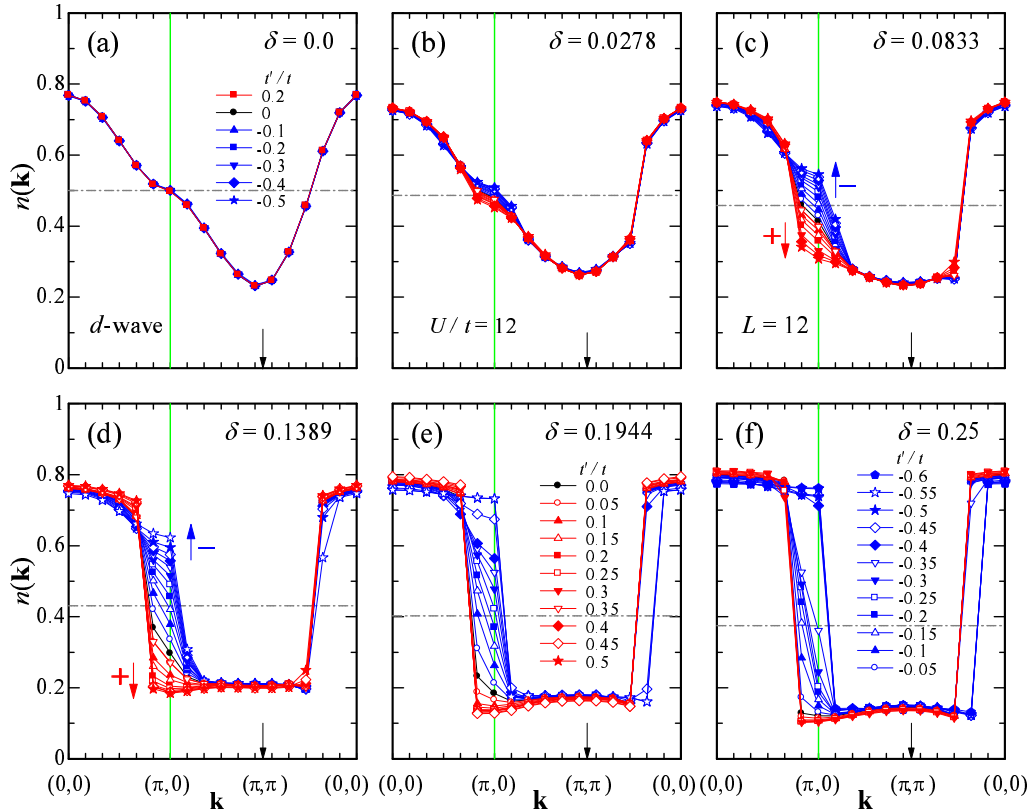


**Fig. 29.** (Color online) Momentum distribution function of  $d$ -wave state for various values of  $t'/t$  for  $U/t = 12$  and  $L = 12$ ; the behavior basically does not alter if  $U/t$  ( $\gtrsim 10$ ) or  $L$  varies. The doping rate is varied among the panels. The symbols for  $t'/t$  instructed in (a), (e) and (f) are common to all panels. Owing to the boundary condition,  $k_y$  for each  $\mathbf{k}$ -point shifts by  $\pi/(2L)$ . The arrows with  $+$  [ $-$ ] in (c) and (d) indicate the direction of variation for  $t'/t > 0$  [ $t'/t < 0$ ] when  $|t'/t|$  increases; this  $t'/t$  dependence does not alter for (b), (e) and (f). The  $(\pi,0)$  point is marked with a vertical guide line, and the  $(\pi,\pi)$  point with a small arrow on the abscissa.



around the antinodal point seems relevant.<sup>44,123)</sup> The maximum of  $|\nabla n(\mathbf{k})|$  is often used as an index of a quasi Fermi surface, and is reduced to a pure Fermi surface for  $|\nabla n(\mathbf{k})| \rightarrow \infty$ . Here, we estimate  $|\nabla n(\mathbf{k})|$  near  $\mathbf{k} = (\pi, 0)$  (abbreviated as  $|\nabla n(\mathbf{X})|$ ) from the finite-size VMC data as follows:  $\partial n(\mathbf{k})/\partial k_x$  and  $\partial n(\mathbf{k})/\partial k_y$  are obtained from finite differences of  $n(\mathbf{k})$  between  $\mathbf{X}'$  and  $\mathbf{X}$  given in §4.3, and those between  $\mathbf{X}$  and  $\mathbf{X}'' = \pi(1, \frac{3}{L})$ , respectively.

In Fig. 31, we plot  $n(\mathbf{k})$  for various  $\delta$ 's ( $L = 10-16$ ) for three values of  $t'/t$  at  $U/t = 12$ . In contrast to the  $t'/t$  dependence [Fig. 29], an appreciable variation exists at any value of  $\mathbf{k}$ , but the magnitude of variation in the antinodal area is still relatively large. We estimate  $|\nabla n(\mathbf{X})|$  for each  $\delta$  from Figs. 31(a)-(c), and plot it as a function of  $\delta$  with a triangle in Figs. 31(d)-(f), respectively, where  $\delta$  dependence of  $P_d^\infty$  is displayed with circles together. For  $t' = 0$ , the behavior of  $|\nabla n(\mathbf{X})|$  closely agrees with that of  $P_d^\infty$  except near half filling, where, however, the disagreement obviously stems from the system-size dependence.<sup>130)</sup> Thus,  $|\nabla n(\mathbf{X})|$  is almost proportional to  $P_d^\infty$  for  $t' = 0$ . For  $t'/t = 0.2$ , the behavior of  $|\nabla n(\mathbf{X})|$  is also nearly proportional to that of  $P_d^\infty$ ;  $|\nabla n(\mathbf{X})|$  exhibits similar system-size dependence near half filling. For  $t'/t = -0.25$ , the overall tendency of  $|\nabla n(\mathbf{X})|$  coincides with that of  $P_d^\infty$ .

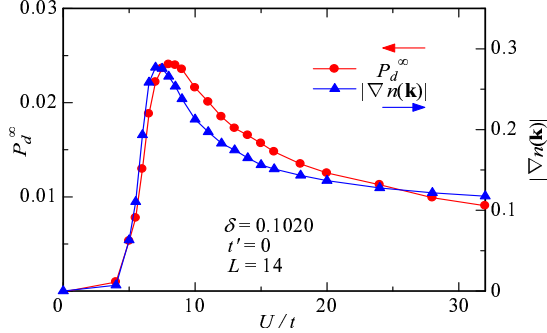


**Fig. 32.** (Color online) Comparison between SC correlation function  $P_d^\infty$  and  $|\nabla n(\mathbf{k})|$  at  $\mathbf{k} = \mathbf{X}' \sim (\pi, 0)$  as function of  $U/t$  for  $t' = 0$  and  $\delta = 0.102$ . The scales of the two quantities are adjusted so as to roughly equalize the maximum magnitudes.

Finally, we touch on the  $U/t$  dependence of  $|\nabla n(\mathbf{X})|$ . If the simple  $d$ -wave BCS function without correlation factors is used, we have  $|\nabla n(\pi, 0)| = 0$  by differentiating

$$n(\mathbf{k}) = |v_{\mathbf{k}}|^2 = \frac{1}{2} \left[ 1 - \frac{\varepsilon_{\mathbf{k}} - \zeta}{\sqrt{(\varepsilon_{\mathbf{k}} - \zeta)^2 + \Delta_{\mathbf{k}}^2}} \right], \quad (28)$$

so that finite  $|\nabla n(\mathbf{X})|$  is considered as a correlation effect. Figure 32 compares  $|\nabla n(\mathbf{X})|$  and  $P_d^\infty$  of  $\Psi_Q^d$  for  $t' = 0$  as a function of  $U/t$  in a slightly underdoped electron density. The two quantities are both almost zero for  $U/t \lesssim 4$ , and broadly agree for any  $U/t$ , suggesting that the electron distribution near  $(\pi, 0)$  is important for  $d$ -wave SC irrespective of the correlation strength.

In this section, we have demonstrated that the strength of SC,  $P_d^\infty$ , behaves similarly to  $|\nabla n(\mathbf{X})|$  near

regarding the stability of the  $d$ -wave state in previous sections, and is consistent with recent experiments,<sup>32,93)</sup> which argue that the antinodal electrons contribute to the SC gap. On the other hand, this result is contradictory to the concept of the dichotomy of electronic roles in the wave-number space, in which electrons near the nodal direction contribute to SC, and electrons near the antinodal point exclusively to the pseudogaps.<sup>23,24)</sup> Similar results were recently obtained by extended methods of DMFT.<sup>131,132)</sup>

## 6. Summary

With the high- $T_c$  cuprates in mind, we studied  $U/t$ ,  $\delta$  and  $t'/t$  dependence of a correlated  $d_{x^2-y^2}$ -wave singlet state  $\Psi_Q^d$  and an antiferromagnetic (AF) state  $\Psi_Q^{\text{AF}}$  independently as doped Mott insulators, applying them to a two-dimensional Hubbard ( $t$ - $t'$ - $U$ ) model. The expectation values are calculated using a variational Monte Carlo method without additional approximations. Main results are recapitulated below.

(1) As  $U/t$  increases,  $\Psi_Q^d$  undergoes a sharp crossover of SC properties from a conventional BCS type to a kinetic-energy-driven type at  $U = U_{\text{co}}$  somewhat larger than the band width ( $8t$ ). As  $\delta$  decreases,  $U_{\text{co}}$  continuously connected to the Mott transition point  $U_c$  at half filling. For  $U < U_{\text{co}}$ , superconductivity (SC), which is fragile, is enhanced by the pair scattering of the vector  $\mathbf{Q} = (\pi, \pi)$  near the antinodes, according to the ordinary  $d$ -wave BCS theory. For  $U/t \lesssim 5$ , steady SC corresponding to the high- $T_c$  cuprates is not found. The SC correlation function  $P_d^\infty$  abruptly increases for  $U/t \gtrsim 6$ . The unconventional SC for  $U > U_{\text{co}}$  is robust for a wide range of  $t'/t$  and  $\delta$ , which coincides with the range where the doublon-holon binding correlation—the essence of Mott physics—is effective, and the picture of the  $t$ - $J$  model is valid. This SC cannot be understood by the instability of the Fermi surface in the underlying normal state.

(2) By comparing the  $\delta$  dependence of  $d$ -wave SC correlation function  $P_d^\infty$  with the dome shape of  $T_c$  and the condensation energy experimentally observed in the cuprates, we showed that the effective value of  $U$  for the cuprates must be larger than at least the Mott critical value  $U_c$  ( $\sim 7t$ ). Furthermore, we found from the analysis of kinetic energy that there are two kinds of holons for  $U > U_{\text{co}}$ ; a holon created during a doublon formation does not contribute to conduction, but a holon introduced by doping becomes a carrier. Consequently, the number of doped holes (electrons) becomes equal to the carrier number. This is a natural picture in the  $t$ - $J$  model, and consistent with various experimental results of cuprates.<sup>116,117)</sup> On the other hand, for  $U < U_{\text{co}}$ , all the holons (electrons) work in the same way as carriers, which make an ordinary large Fermi surface. This Fermi-liquid feature is contradictory to that of the cuprates.

(3) In view of the two gap problem, the present result for  $U > U_c$  is interpreted as follows: A gap for the singlet pair formation  $\Delta_d$ , which possibly corresponds to a pseudogap, is a decreasing function of  $\delta$ . Meanwhile, the strength of SC represented by  $P_d^\infty$  (related to the SC gap) has a dome-shaped  $\delta$  dependence, and is written by the



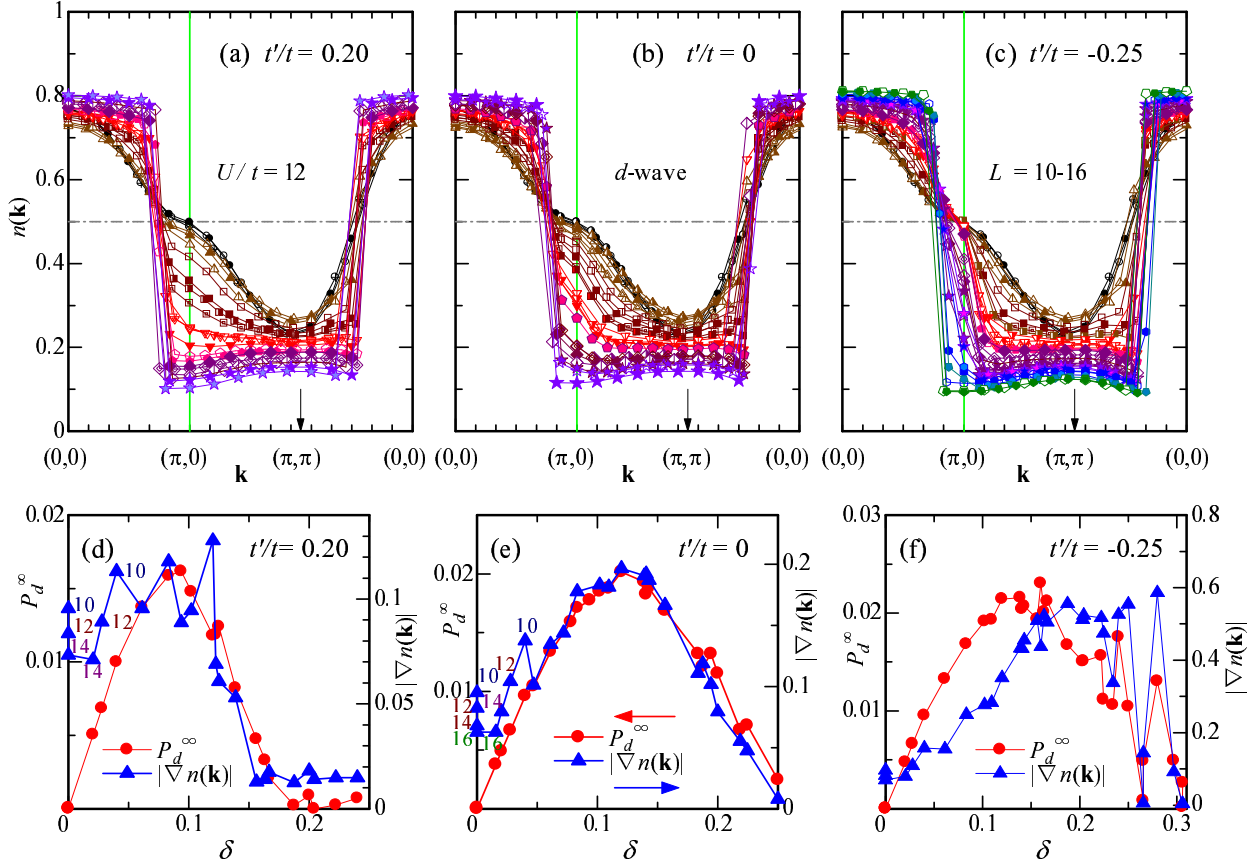


**Fig. 31.** (Color online) (a)-(c) Momentum distribution function of  $\Psi_Q^d$  for various values of  $\delta$  at  $U/t = 12$ . The value of  $t'/t$  is varied among the three panels. The data for  $L = 10-16$  are simultaneously displayed. Detailed instruction for  $\delta$  is omitted, but circles denote  $\delta = 0$ , upward triangles  $\delta = 0.02-0.04$ , squares  $\delta = 0.06-0.11$ , downward triangles  $\delta = 0.12-0.14$ , upward pentagons  $\delta = 0.15-0.165$ , diamonds  $\delta = 0.165-0.21$ , stars  $\delta = 0.22-0.25$ , hexagons  $\delta = 0.26-0.29$ , and downward pentagons  $\delta = 0.29-0.31$ . To adjust the scale in the section  $(0,0)-(\pi,0)-(\pi,\pi)$ , the locus of  $\mathbf{k}$  points between  $(\pi,\pi)-(0,0)$  slightly shifts depending on  $L$ . (d)-(f) Comparison between SC correlation function  $P_d^\infty$  and  $|\nabla n(\mathbf{k})|$  near  $\mathbf{k} = (\pi,0)$  estimated from the data in (a)-(c) for the three  $t'/t$ 's. We adjust the scales of the two quantities so as to roughly equalize the maximum magnitudes. The small digits for  $\delta \sim 0$  in (d) and (e) indicate the system size  $L$  used for the corresponding data point.

bility such as the carrier density and the quasiparticle renormalization factor  $Z$ , which are increasing functions of  $\delta$  for small  $\delta$ . This suppression of charge fluctuation is imposed by the Mott physics. This feature of the SC gap is consistent with various theories for the  $t$ - $J$  model.

(4) A proper negative (positive)  $t'/t$  term stabilizes the SC (AF) state and destabilizes the AF (SC) state. A case of a very small  $\delta$  and a quite large  $U/t$  is exceptional. Meanwhile, the AF state is intrinsically unstable for hole-doped cases ( $t'/t \lesssim 0$ ), and phase separates to the AF state with the local electron density  $n = 1$  and the SC state with  $n < 0.85$ .

(5) For the stability of AF state, the nesting of  $\mathbf{Q}$  is primarily important on the whole Fermi surface. On the other hand, crucial for SC is the pair scattering of  $\mathbf{Q}$  in the antinodal area, where the underlying band is flat. To check this aspect, we showed that the SC correlation  $P_d^\infty$  is closely connected to the slope of momentum distribution function  $|\nabla n(\mathbf{k})|$  near the antinodal point. This contradicts the often argued dichotomy of electronic roles in the  $\mathbf{k}$  space, i.e. the electrons in the nodal (antinodal) area exclusively contribute to SC (pseudogap).

Finally, we briefly mention some future problems. (i) It

is important to include long-range hopping terms in the band dispersion and the band renormalization effects owing to the electron correlation. (ii) We should check the coexistence of SC and AF orders and their mutual exclusion. (iii) In connection with the pseudogap problem, normal states with some symmetry breakings should be studied. (iv) Making the most use of recent progress in VMC techniques,<sup>133)</sup> we have to explore more exquisite trial wave functions.<sup>114, 134)</sup> (vi) We should study the role of doublons and holons in the SC phase more in detail, for instance, to check a recent proposal.<sup>135)</sup>

## Acknowledgments

The authors thank Tsutomu Watanabe and Takafumi Sato for useful discussions. This work is partly supported by Grant-in-Aids from the Ministry of Education, Culture, Sports, Science and Technology.

## Appendix A: Hubbard model for cuprates

To consider the  $\text{CuO}_2$  planes, a proper starting model is the  $d$ - $p$  model composed of  $\text{O-}2p$  and  $\text{Cu-}3d_{x^2-y^2}$  orbitals. The  $d$ - $p$  model is reducible to more simple models which still capture the essence of  $\text{CuO}_2$  planes. Since a

**Table B.1.** Absolute values of total energy of the  $d$ -wave state,  $|E/t|$ , are compared among the three D-H correlation factors for  $\delta > 0$ ,  $t'/t = 0$  and  $L = 10$ . The last digits may have some errors.

$\delta$	0.20			0.12		
$U/t$	$\mathcal{P}_Q^D$	$\mathcal{P}_Q^S$	$\mathcal{P}_Q^{DH}$	$\mathcal{P}_Q^D$	$\mathcal{P}_Q^S$	$\mathcal{P}_Q^{DH}$
4	1.0754	1.0773	1.0773	0.9914	0.9935	0.9935
6	0.9237	0.9282	0.9284	0.7979	0.8035	0.8038
8	0.8216	0.8288	0.8291	0.6750	0.6841	0.6854
10	0.7545	0.7626	0.7634	0.6010	0.6094	0.6121
12	0.7084	0.7165	0.7177	0.5518	0.5583	0.5624
16	0.6502	0.6576	0.6591	0.4903	0.4936	0.4988

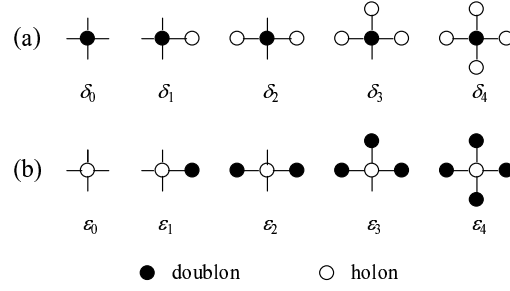


**Fig. B.1.** (a) Local configurations around a doublon are classified according to the number of holons in the nearest-neighbor sites. (b) A similar classification around a holon.

doped electron enters a  $\text{Cu-}3d_{x^2-y^2}$  orbital, the model is reduced to a Hubbard model on a square lattice by eliminating the degree of freedom for the  $\text{O-}2p$  orbitals. In contrast, a doped hole enters an  $\text{O-}2p$  orbitals; a Zhang-Rice singlet is formed, through which the model for low dopant density is reduced to the  $t$ - $J$  model on a square lattice with small  $J/t$ .<sup>2)</sup> This  $t$ - $J$  model is connected to the Hubbard model with large  $U/t$  ( $= 4t/J$ ) through the strong-coupling expansion<sup>136)</sup> within the approximation of neglecting the pair-hopping (three-site) terms. Thus, the Hubbard model on a square lattice is derived as an effective model for both in electron-doped (ED) and hole-doped (HD) cuprates. Note, however, that the effective value of  $U/t$  in the Hubbard model may differ between ED and HD cases owing to the distinct derivation paths, even if the actual values of  $U$  in the  $\text{Cu-}3d_{x^2-y^2}$  orbitals are identical between the two.

Another vital element of the model, eq. (1), is that one can map a more-than-half-filled case ( $n > 1$ ) to a less-than-half-filled case ( $n < 1$ ) by taking advantage of the antisymmetric level structure with respect to  $n = 1$ . The band dispersion, eq. (2), for  $\tilde{\mathbf{k}} = (\pi - k_y, \pi - k_x)$ , which is the symmetric point of  $\mathbf{k}$  with respect to the Fermi surface at half filling for  $t' = 0$  (AF Brillouin zone boundary), is written as,

$$\tilde{\varepsilon}(\tilde{\mathbf{k}}) = 2\tilde{t}(\cos k_x + \cos k_y) - 4\tilde{t}' \cos k_x \cos k_y, \quad (\text{A.1})$$

where tildes are the marks for  $\tilde{\mathbf{k}}$ . To satisfy  $\varepsilon(\mathbf{k}) = -\tilde{\varepsilon}(\tilde{\mathbf{k}})$ , we need the relations  $\tilde{t} = t$  and  $\tilde{t}' = -t'$ , which are represented by a canonical (electron-hole) transformation,

$$c_{i\sigma}^\dagger \rightarrow e^{i\mathbf{Q} \cdot \mathbf{r}_i} \tilde{c}_{i\sigma}, \quad (\text{A.2})$$

with  $\mathbf{Q} = (\pi, \pi)$ . Under this transformation, the model eq. (1) is invariant except for the addition of a constant  $U(N_s - N)$ . Consequently, calculations for an ED system with electron density  $n = 1 + \delta$  ( $\delta > 0$ ) and  $t'/t$  ( $< 0$ ) can be replaced by those for the less-than-half-filled case with  $1 - \delta$  and  $|t'/t|$ , if we consider  $t'/t$  is negative for both ED and HD cuprates.

## Appendix B: Details of doublon-holon factors

In this Appendix, we compare different forms of the D-H correlation factor  $\mathcal{P}_Q$  [eq.(5)] to show that the difference in results among  $Q_j^D$  [eq. (7)] and other forms of  $Q_j$  is insignificant. Here,  $\mathcal{P}_Q$  between nearest-neighbor sites is mainly considered, because  $\mathcal{P}_Q$  between further sites only make a minor difference.<sup>20)</sup>

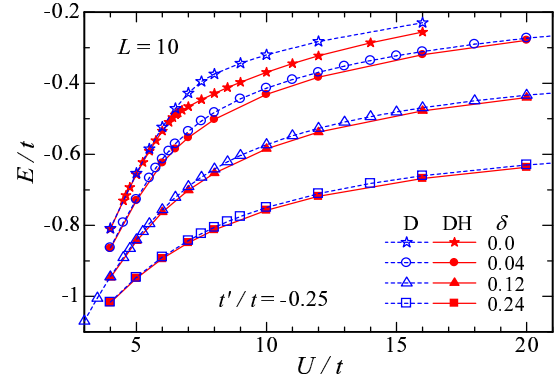


**Fig. B.2.** (Color online) The total energy of  $\Psi_j^d$  with  $\mathcal{P}_Q^{DH}$  (solid symbols) is compared with that with  $\mathcal{P}_Q^D$  (open symbols) as a function of  $U/t$  for four  $\delta$ 's. At half filling,  $Q_j^{DH}$  is reduced to  $Q_j^S$  (solid stars).<sup>17)</sup> Tendency for other values of  $t'/t$  is similar.

[eq. (6)] ( $\mathcal{P}_Q^S$ ) have been used,<sup>80, 81, 137)</sup> on account of the particle-hole or doublon-holon symmetry. For  $\delta > 0$ , however, this symmetry is broken, and the number of holons always exceeds that of doublons. Consequently, if  $\mathcal{P}_Q^S$  is used, configurations  $\delta_2$ ,  $\delta_3$  and  $\delta_4$  illustrated in Fig. B.1 seem to appear frequently as  $\delta$  increases. In fact, a recent study<sup>123)</sup> using a detailed parameterization for  $Q_j$  has revealed that such configurations rarely appear for large  $U/t$ , because they increase the interaction energy  $Ud$ . Anyway, we consider another asymmetric form of  $Q_j$ , which is a natural extension of  $Q_j^S$ :

$$Q_j^{DH} = \mu_d d_j \prod_{\tau} (1 - h_{j+\tau}) + \mu_h h_j \prod_{\tau} (1 - d_{j+\tau}), \quad (\text{B.1})$$

where binding parameters for holons  $\mu_h$  and doublons  $\mu_d$  are optimized independently. At half filling,  $Q_j^{DH}$  is reduced to  $Q_j^S$  ( $\mu_h = \mu_d$ ) to retrieve the symmetry. As  $\delta$  increases,  $\mu_h$  is expected to decrease much faster than  $\mu_d$  because  $\varepsilon_2$  comes to appear less frequently than  $\delta_2$ ; therefore  $Q_j^{DH}$  approaches  $Q_j^D$  ( $\mu_h$  rapidly decreases). As shown in Table B.1,<sup>138)</sup> the variational energy of  $Q_j^{DH}$  is improved on that of  $Q_j^S$ , especially for large  $U/t$ . In the following, we compare asymmetric forms  $Q_j^{DH}$  and  $Q_j^D$ .

In Fig. B.2, the total energy of the  $d$ -wave state is compared between  $Q_j^D$  and  $Q_j^{DH}$  for  $t'/t = -0.25$ . In Table B.2, we list the energy improvement by  $Q_j^{DH}$  on

**Table B.2.** Improvement of total energy by  $\Psi_Q^{\text{DH}}$  on  $\Psi_Q^{\text{D}}$  in percentage,  $(E^{\text{D}} - E^{\text{DH}})/|E^{\text{D}}| \times 100$ , for various parameter values and  $L = 10$ , which satisfy the closed-shell condition.

$t'/t$	-0.25				0			
$\delta$	0.24	0.12	0.04	0.0	0.20	0.12	0.04	0.0
$U/t$								
4	0.2	0.2	0.2	0.2	0.2	0.2	0.2	0.3
6	0.5	1.0	1.8	2.0	0.5	0.7	1.5	1.9
8	0.8	1.8	4.1	14.6	0.9	1.5	3.9	14.0
10	1.0	2.0	4.2	15.3	1.2	1.8	4.0	15.0
12	1.1	2.0	3.7	14.3	1.3	1.9	3.7	14.0
16	1.2	1.8	2.8	11.4	1.4	1.7	2.7	11.3

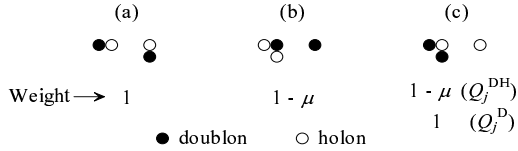


**Fig. B.3.** Weight assignment by  $Q_j^{\text{DH}}$  and by  $Q_j^{\text{D}}$  to local configurations with two doublons and two holons typical for  $U \sim U_{\text{co}}$  at half filling. All the sites in the background are singly occupied. In each case, only relative positions of doublons to holons are illustrated. In (a), there are two  $\delta_1$  and two  $\varepsilon_1$ ; in (b),  $\delta_2$ ,  $\delta_0$  and two  $\varepsilon_1$ ; and in (c),  $\varepsilon_2$ ,  $\varepsilon_0$  and two  $\delta_1$ .

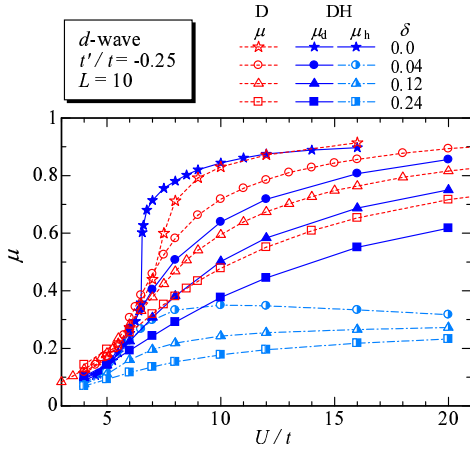


**Fig. B.4.** (Color online) Comparison of optimized D-H correlation parameters between  $Q_j^{\text{D}}$  ( $\mu$ ) and  $Q_j^{\text{DH}}$  ( $\mu_d$  and  $\mu_h$ ) for nearest-neighbor sites.

$Q_j^{\text{D}}$  ( $\Delta E = E^{\text{D}} - E^{\text{DH}}$ ) for some values of  $\delta$  and  $t'/t$  as a function of  $U/t$ . In every case, the energy is improved by  $Q_j^{\text{DH}}$ . Comparing  $\Delta E/t$  for  $t'/t = -0.25$  and 0, we find that  $\Delta E$  only slightly depends on  $t'/t$ . For each  $\delta$ ,  $\Delta E/t$  has a maximum near  $U_{\text{co}}/t = 10$ , especially at half filling,  $Q_j^{\text{DH}} (=Q_j^{\text{S}})$  becomes highly advantageous for  $U > U_c$ . For a fixed  $U/t$ ,  $\Delta E/t$  decreases as  $\delta$  increases.

We briefly consider the reason why  $Q_j^{\text{DH}}$  is advantageous at half filling and for  $U \sim U_{\text{co}}$ . Assume that only two doublons and two holons exist in a local electron configurations at half filling; typical ones frequently appearing for  $U \sim U_{\text{co}}$  are shown in Fig. B.3. The Gutzwiller factor assigns a common weight  $g^2$  to each of these configurations. As for the D-H factors,  $\mathcal{P}_Q^{\text{DH}}$  and  $\mathcal{P}_Q^{\text{D}}$  give the same weights 1 and  $1 - \mu$  for the configurations (a) and

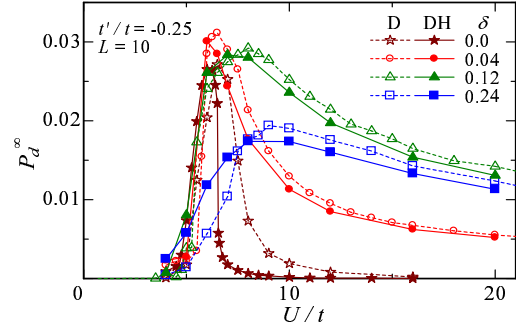


**Fig. B.5.** (Color online) Comparison of  $d$ -wave pair correlation function between two D-H correlation factors,  $\mathcal{P}_Q^{\text{DH}}$  and  $\mathcal{P}_Q^{\text{D}}$ . The behavior of  $P_d^{\infty}$  is similar for other values of  $t'/t$ .

(b), respectively;<sup>123</sup> however, for an unfavorable configuration (c),  $\mathcal{P}_Q^{\text{D}}$  gives 1, but  $\mathcal{P}_Q^{\text{DH}}$  reduces the weight as  $1 - \mu$ . Thus,  $Q_j^{\text{DH}}$  becomes better than  $Q_j^{\text{D}}$  at  $\delta = 0$  and for  $U \sim U_{\text{co}}$ . When holes are doped, configurations like  $\varepsilon_2$  (also  $\varepsilon_3$  and  $\varepsilon_4$ ) appearing in Fig. B-3(c) are rapidly suppressed; accordingly, the difference between  $Q_j^{\text{HD}}$  and  $Q_j^{\text{D}}$  narrows. This aspect is clearly seen in the optimized D-H binding factors  $\mu$  in  $Q_j^{\text{D}}$  and  $\mu_d$  and  $\mu_h$  in  $Q_j^{\text{DH}}$ , as shown in Fig. B.4. As  $\delta$  increases,  $\mu_d$  becomes slightly small, but  $\mu_h$  considerably and rapidly decreases, compared with  $\mu$  in  $Q_j^{\text{D}}$  denoted by open symbols.

Because the optimized values of the other variational parameters are similar between the two cases of  $\mathcal{P}_Q^{\text{DH}}$  and  $\mathcal{P}_Q^{\text{D}}$  (not shown), physical quantities, e.g.  $n(\mathbf{k})$ ,  $S(\mathbf{q})$  and  $N(\mathbf{q})$ , thereof becomes similar (not shown). Among them, the  $d$ -wave pairing correlation function exhibit a relatively large difference as shown in Fig. B-5; the maximum of  $P_d^{\infty}$  is located at a slightly smaller  $U/t$  for  $Q_j^{\text{DH}}$ . However, the difference remains within quantitative.

In conclusion, the D-H correlation factor  $\mathcal{P}_Q^{\text{D}}$  possesses properties sufficiently close to those of an improved factor  $\mathcal{P}_Q^{\text{DH}}$  at least for  $\delta > 0$ .

### Appendix C: Pairing correlation function

We explain the details of how we determine long-distance values ( $P_d^{\infty}$ ) of the  $d_{x^2-y^2}$ -wave SC correlation function  $P_d(\mathbf{r})$  defined by eq. (20) with eq. (21), to avoid misunderstanding. If  $P_d(\mathbf{r})$  remains finite for  $|\mathbf{r}| \rightarrow \infty$ , an off-diagonal long-range order exists. For finite systems, however, one must be careful to estimate the value of  $P_d(\mathbf{r})$  for  $|\mathbf{r}| = \infty$ .

In Fig. C-1, the behavior of  $P_d(\mathbf{r})$  for the noninteracting case ( $U/t = 0$ ) is compared among different system sizes. Here, the path of  $\mathbf{r}$  is chosen as shown in Fig. C-2(c). Because SC does not occur for  $U/t = 0$ ,  $P_d(\mathbf{r})$  must vanish for large  $|\mathbf{r}|$ . However, for small systems like  $L = 10$  and 12,  $P_d(\mathbf{r})$  still has appreciable magnitude at distant points, e.g.  $\mathbf{r} = (L/2, 0)$  and  $\mathbf{r} = (L/2, L/2)$ . Furthermore, the location of large magnitude of  $P_d(\mathbf{r})$  depends on the values of  $t'/t$  and  $\delta$ . If we require that  $P_d(\mathbf{r})$  should vanish for every distant point in this scale, we need to use a system with  $L \gtrsim 30$ . Such tendency remains for fairly large values of  $U/t$ , as seen in Fig. C-2. Fortunately, we found that  $P_d(\mathbf{r})$  for  $\mathbf{r} = (L/2, 0)$  and  $\mathbf{r} = (L/2, L/2)$

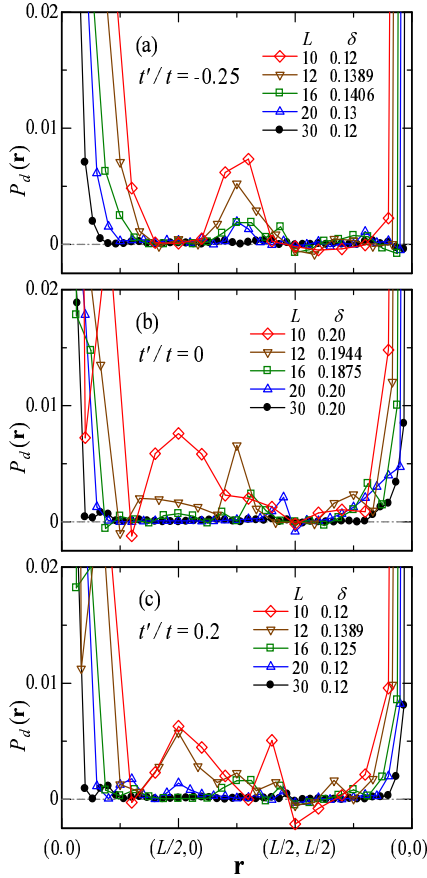


**Fig. C.1.** (Color online) System-size dependence of  $d$ -wave SC correlation function  $P_d(\mathbf{r})$  for noninteracting systems ( $U/t = 0$ ). The path of  $\mathbf{r}$  is illustrated in Fig. C.2(c). The values of  $t'/t$  and  $\delta$  are (a)  $-0.25$  and  $\sim 0.13$ , (b)  $0$  and  $\sim 0.20$ , and (c)  $0.2$  and  $\sim 0.13$ , respectively.  $\delta$  is chosen so as to satisfy the closed-shell condition under the same boundary condition as that in the VMC calculations. The data are obtained using the analytic formula.

which is next to the farthestmost point, is substantially zero (less than  $10^{-4}$ ) at  $U = 0$  regardless of the values of  $t'/t$ ,  $\delta$  and  $L$ , and remains smaller than those for  $\mathbf{r} \neq \mathbf{r}_\infty$  for small  $U/t$ . Hence, we employ  $P_d(\mathbf{r}_\infty)$  as  $P_d^\infty$  for small  $U/t$  ( $0 \leq U \leq U_{\max}$ ), where  $U_{\max}$  indicates the value of  $U$  of the largest  $P_d(\mathbf{r})$  for a fixed  $t'/t$ . Thereby, the artificial enhancement of  $P_d(\mathbf{r})$  owing to the finite sizes can be eliminated.

For large  $U/t$  ( $U > U_{\max}$ ),  $P_d^\infty$  can be determined more confidently.  $U/t$  dependence of  $P_d(\mathbf{r})$  for fixed  $L$  and  $\delta$  is shown in Fig. C.2.  $P_d(\mathbf{r})$  exhibits finite-size fluctuations for  $U \lesssim U_{\max}$ , but becomes almost constant for  $|\mathbf{r}| \geq 3^{139}$  regardless of  $t'/t$  and  $L$  for  $U \gtrsim U_{\max}$ . This behavior is the same as that found for the  $t$ - $J$  model,<sup>51)</sup> and reflects the short-range nature of strong correlation. Thus, we use the average value of  $P_d(\mathbf{r})$  for  $|\mathbf{r}| \geq 3$  as  $P_d^\infty$  for  $U > U_{\max}$ .

In summary, as a proper indicator of  $d$ -wave SC order, we safely define the long-distance value of  $P_d(\mathbf{r})$  for finite

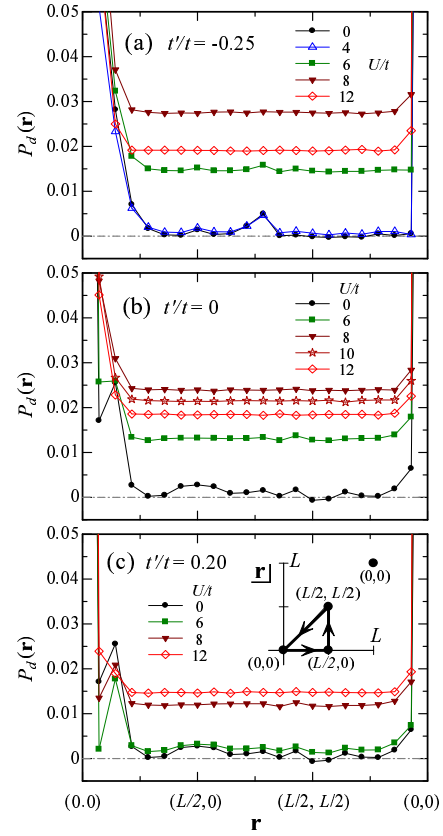


**Fig. C.2.** (Color online)  $U/t$  dependence of  $d$ -wave SC correlation function  $P_d(\mathbf{r})$  for  $L = 14$  and  $\delta = 0.102$ . The path of  $\mathbf{r}$  is depicted in (c);  $\mathbf{r}_\infty$  is not on this path. The value of  $t'/t$  is (a)  $-0.25$  (hole doped), (b)  $0$ , and (c)  $0.2$  (electron doped). In these systems,  $U_{\max}/t = 8.0, 8.1$  and  $10.5$  for  $t'/t = -0.25, 0$  and  $0.2$ , respectively. In every case, the closed-shell condition is satisfied. Note that the scale of the vertical axis is larger than Fig. C.1. The data are obtained using the analytic formula for  $U/t = 0$ , and VMC otherwise.

systems by,

$$P_d^\infty = \begin{cases} P_d(\mathbf{r}_\infty) & (U < U_{\max}) \\ \frac{1}{M} \sum_{|\mathbf{r}_j| \geq 3} P_d(\mathbf{r}_j) & (U \geq U_{\max}) \end{cases}, \quad (\text{C.1})$$

where  $\mathbf{r}_\infty = (L/2 - 1, L/2)$ , and  $M$  is the number of vectors  $\mathbf{r}_j$  satisfying  $|\mathbf{r}_j| \geq 3$ .

- 1) P.W. Anderson: Science **235** (1987) 1196.
- 2) F. C. Zhang and T. M. Rice: Phys. Rev. B **37** (1988) 3759.
- 3) For instance, D. J. Scalapino, Phys. Rep. **250** (1995) 329; P. W. Anderson *et al.*: J. Phys. Cond. Mat. **16** (2004) R755.
- 4) P. A. Lee, N. Nagaosa and X. -G. Wen: Rev. Mod. Phys. **78** (2006) 17.
- 5) M. Ogata and H. Fukuyama: Rep. Prog. Phys. **71** (2008) 036501.
- 6) For instance, T. Moriya and K. Ueda: Adv. Phys. **49** (2000) 555; Y. Yanase *et al.*: Phys. Rep. **387** (2003) 1; H. Kontani, K. Kanki and K. Ueda: Phys. Rev. B **59** (1999) 14723.
- 7) C. J. Halboth and W. Metzner: Phys. Rev. B **61** (2000) 7364; D. Zanchi and H.J. Schulz: Phys. Rev. B **61** (2000) 13609; N. Furukawa, T.M. Rice and N. Salmhofer: Phys. Rev. Lett. **81** (1998) 3195.

- M. Imada: J. Phys. Soc. Jpn. **61** (1992) 3331; K. Kuroki and H. Aoki: Phys. Rev. B **56** (1997) R14287; M. Guerrero, G. Ortiz and J. E. Gubernatis: Phys. Rev. B **59** (1999) 1706.
- 9) T. Aimi and M. Imada: J. Phys. Soc. Jpn. **76** (2007) 113708.
  - 10) T. Yanagisawa: J. Phys. Soc. Jpn. **79** (2010) 063708.
  - 11) W. L. McMillan, Phys. Rev. **138** (1965) A442.
  - 12) D. Ceperley, G. V. Chester, K. H. Kalos, Phys. Rev. B **16** (1977) 3081.
  - 13) H. Yokoyama and H. Shiba: J. Phys. Soc. Jpn. **57** (1988) 2482.
  - 14) C. Gros: Ann. Phys. (New York) **189** (1989) 53.
  - 15) H. Yokoyama and M. Ogata: J. Phys. Soc. Jpn. **65** (1996) 3615.
  - 16) H. Yokoyama, Y. Tanaka, M. Ogata and H. Tsuchiura: J. Phys. Soc. Jpn. **73** (2004) 1119.
  - 17) H. Yokoyama, M. Ogata and Y. Tanaka: J. Phys. Soc. Jpn. **75** (2006) 114706.
  - 18) M. Ogata, H. Yokoyama, Y. Yanase, Y. Tanaka, and H. Tsuchiura: J. Phys. Chem. Solids **67** (2006) 37.
  - 19) H. Yokoyama, Y. Tanaka and M. Ogata: J. Phys. Chem. Solids **67** (2006) 47.
  - 20) T. Miyagawa and H. Yokoyama: J. Phys. Soc. Jpn. **80** (2011) 084705, and Physica C **471** (2011) 738.
  - 21) H. Yokoyama, T. Miyagawa, and M. Ogata: J. Phys. Soc. Jpn. **80** (2011) 084607, and Physica C **471** (2011) 730.
  - 22) M. Imada, A. Fujimori, and Y. Tokura: Rev. Mod. Phys. **70** (1998) 1039.
  - 23) For instance, G. Deutscher: Nature **397** (1999) 410; A. J. Millis: Science **314** (2006) 1888; S. Hüfner, M. A. Hossain, A. Damascelli and G. A. Sawatzky: Rep. Prog. Phys. **71** (2008) 062501.
  - 24) T. Yoshida, M. Hashimoto, I. M. Vishik, Z. -X. Shen, and A. Fujimori: J. Phys. Soc. Jpn. **81** (2012) 011006.
  - 25) M. Le Tacon *et al.*: Nat. Phys. **2** (2006) 537.
  - 26) K. Tanaka *et al.*: Science **314** (2006) 1910; T. Kondo, T. Takeuchi, A. Kaminski, S. Tsuda, and S. Shin: Phys. Rev. Lett. **98** (2007) 267004.
  - 27) M. Hashimoto *et al.*: Phys. Rev. B **75** (2007) 140503.
  - 28) M. C. Boyer *et al.*: Nat. Phys. **3** (2007) 802.
  - 29) Y. Wang, L. Li, and N. P. Ong: Phys. Rev. B **73** (2006) 024510.
  - 30) A. Kanigel *et al.*: Nat. Phys. **2** (2006) 447.
  - 31) T. Valla, A. V. Fedorov, J. Lee, J. C. Davis, and G. D. Gu: Science **314** (2006) 1914.
  - 32) K. Terashima *et al.*: Phys. Rev. Lett. **99** (2007) 017003; M. Shi *et al.*: Phys. Rev. Lett. **101** (2008) 047002, and Europhys. Lett. **88** (2009) 27008.
  - 33) J. -H. Ma *et al.*: Phys. Rev. Lett. **101** (2008) 207002.
  - 34) T. Yoshida *et al.*: Phys. Rev. Lett. **103** (2009) 037004.
  - 35) K. Nakayama *et al.*: Phys. Rev. B **83** (2011) 224509.
  - 36) L. Yu *et al.*: Phys. Rev. Lett. **100** (2008) 177004.
  - 37) A. Dubroka *et al.*: Phys. Rev. Lett. **106** (2011) 047006.
  - 38) R. Daou *et al.*: Nature **463** (2010) 519.
  - 39) M. J. Lawler, *et al.*: Nature **466** (2010) 347; A. Mesaros, *et al.*: Science **333** (2011) 426.
  - 40) K. K. Gomes *et al.*: Nature **447** (2007) 569.
  - 41) Y. Kohsaka *et al.*: Nat. Phys. **8** (2012) 534.
  - 42) K. Fujita *et al.*: J. Phys. Soc. Jpn. **81** (2012) 011005.
  - 43) H. -B. Yang *et al.*: Nature **456** (2008) 77.
  - 44) H. Yokoyama, M. Ogata, and K. Kobayashi: Physica C **470** (2010) S149.
  - 45) H. Yokoyama, S. Tamura, T. Miyagawa, K. Kobayashi, and M. Ogata: Phys. Proc. **27** (2012) 60.
  - 46) T. Tanamoto, H. Kohno, and H. Fukuyama: J. Phys. Soc. Jpn. **61** (1992) 1886.
  - 47) T. Tohyama and S. Maekawa: Phys. Rev. B **49** (1994) 3596; T. Tohyama: Phys. Rev. B **70** (2004) 174517.
  - 48) R. J. Gooding, K. J. E. Vos, and P. W. Leung: Phys. Rev. B **50** (1994) 12866.
  - 49) R. Raimondi, J. H. Jefferson, and L. F. Feiner: Phys. Rev. B **53** (1996) 8774.
  - 50) E. Pavarini *et al.*: Phys. Rev. Lett. **87** (2001) 047003.
  - 51) C. T. Shih *et al.*: Phys. Rev. Lett. **92** (2004) 227002.
  - 52) D. J. Scalapino, E. Loh Jr., and J. E. Hirsch: Phys. Rev. B **34** (1986) 8190; N. E. Bickers, D. J. Scalapino, and R. T. Scalettar, Int. J. Mod. Phys. **B1** (1987) 687; H. Shimahara and S. Takada, J. Phys. Soc. Jpn. **57** (1988) 1044.
  - 53) N. E. Bickers, D. J. Scalapino, and S. R. White, Phys. Rev. Lett. **62** (1989) 961.
  - 54) T. Nomura and K. Yamada, J. Phys. Soc. Jpn. **72** (2003) 2053.
  - 55) R. Hlubina: Phys. Rev. B **59** (1999) 9600; J. Kondo: J. Phys. Soc. Jpn. **70** (2002) 808.
  - 56) E. Dagotto *et al.*: Phys. Rev. B **49** (1994) 3548.
  - 57) S. Sorella *et al.*: Phys. Rev. Lett. **88** (2002) 117002.
  - 58) T. Giamarchi and C. Lhuillier: Phys. Rev. B **43** (1991) 12943.
  - 59) K. Yamaji, T. Yanagisawa, T. Nakanishi, and S. Koike: Physica C **304** (1998) 225.
  - 60) T. Yanagisawa, S. Koike, and K. Yamaji: J. Phys. Soc. Jpn. **68** (1999) 3608; D. Baeriswy, D. Eichenberger, and M. Menteshshavilli: New J. Phys. **11** (2009) 075010.
  - 61) T. A. Maier, M. Jarrell, T. C. Schulthess, P. R. C. Kent, and J. B. White: Phys. Rev. Lett. **95** (2005) 237001.
  - 62) D. Sénéchal, P. -L. Lavertu, M. -A. Marois, and A. -M. S. Tremblay: Phys. Rev. Lett. **94** (2005) 156404.
  - 63) M. Aichhorn, E. Arrigoni, M. Potthoff, and W. Hanke: Phys. Rev. B **74** (2006) 024508.
  - 64) M. Capone and G. Kotliar: Phys. Rev. B **74** (2006) 054513.
  - 65) T. K. Lee and S. Feng: Phys. Rev. B **38** (1988) 11809.
  - 66) A. Himeda and M. Ogata: Phys. Rev. B **60** (1999) R9935.
  - 67) M. Aichhorn, E. Arrigoni, M. Potthoff, and W. Hanke: Phys. Rev. B **74** (2006) 024508; S. S. Kancharla *et al.*: Phys. Rev. B **77** (2008) 184516.
  - 68) T. K. Lee, C. -M. Ho, and N. Nagaosa: Phys. Rev. Lett. **90** (2003) 067001.
  - 69) K. Kobayashi and H. Yokoyama: Physica C **469** (2009) 974.
  - 70) For instance, A. Hosseini *et al.*: Phys. Rev. Lett. **93** (2004) 107003.
  - 71) H. Mukuda *et al.*: Phys. Rev. Lett. **96** (2006) 087001, and J. Phys. Soc. Jpn. **77** (2008) 124706.
  - 72) C. -H. Lee *et al.*: J. Phys. Soc. Jpn. **77** (2008) 073706; S. Shimizu *et al.*: J. Phys. Soc. Jpn. **80** (2011) 043706.
  - 73) H. Mukuda, S. Shimizu, A. Iyo, and Y. Kitaoka: J. Phys. Soc. Jpn. **81** (2012) 011008.
  - 74) M. Fujita *et al.*: J. Phys. Soc. Jpn. **81** (2012) 011007.
  - 75) K. Kobayashi and H. Yokoyama: J. Low Temp. Phys. **117** (1999) 199; A. Himeda and M. Ogata: Phys. Rev. Lett. **88** (2002) 117001.
  - 76) R. Jastrow: Phys. Rev. **98** (1955) 1479.
  - 77) M. C. Gutzwiller: Phys. Rev. Lett. **10** (1963) 159.
  - 78) H. Yokoyama and H. Shiba: J. Phys. Soc. Jpn. **56** (1987) 1490.
  - 79) T. A. Kaplan, P. Horsch, and P. Fulde, Phys. Rev. Lett. **49** (1982) 889.
  - 80) H. Yokoyama and H. Shiba: J. Phys. Soc. Jpn. **59** (1990) 3669.
  - 81) T. Watanabe, H. Yokoyama, Y. Tanaka, and J. Inoue: J. Phys. Soc. Jpn. **75** (2006) 074707.
  - 82) H. Yokoyama: Prog. Theor. Phys. **108** (2002) 59.
  - 83) S. Tamura and H. Yokoyama: J. Phys. Soc. Jpn. **81** (2012) 064718, and Phys. Proc. **27** (2012) 76.
  - 84) In ref. 17, we displayed the data of  $\mu'$  at half filling as twice larger than the correct values in error. The ranges of ordinates in Fig. 4(d) and Fig. 15(c) in ref. 17 must be  $[-0.05, 0.05]$  and  $[0, 0.15]$ , respectively. This does not affect the interpretation of physics.
  - 85) J. P. Bouchaud, A. Georges, and C. Lhuillier: J. Phys. (Paris) **49** (1988) 553.
  - 86) Although we have checked the optimized energies for the homogeneous and extended  $s$  waves, they are never stabilized near half filling. To consider the gap form more precisely, it becomes necessary to include SC correlations with longer Cooper pairs.<sup>88)</sup> According to ref. 88, the optimized gap form somewhat deviates from the simple  $d_{x^2-y^2}$  wave, eq. (11). For electron-doped cases,  $\Delta_{\mathbf{k}}$  exhibits nonmonotonic behavior<sup>89)</sup> in consistent with experiments.<sup>90)</sup> For hole-doped cases,  $\Delta_{\mathbf{k}}$  becomes concave near the node directions, which qualitatively accords with the experiments for Bi2212.<sup>91)</sup>



- 88) T. Watanabe, H. Yokoyama, K. Shigeta, and M. Ogata: *New J. Phys.* **11** (2009) 075011.
- 89) H. Yoshimura and D. S. Hirashima: *J. Phys. Soc. Jpn.* **74** (2005) 712; T. Watanabe, T. Miyata, H. Yokoyama, Y. Tanaka, and J. Inoue: *J. Phys. Soc. Jpn.* **74** (2005) 1942.
- 90) G. Blumberg *et al.*: *Phys. Rev. Lett.* **88** (2002) 107002; H. Matsui *et al.*: *Phys. Rev. Lett.* **95** (2005) 017003.
- 91) H. Ding, *et al.*: *Phys. Rev. B* **54** (1996) R9678; J. Mesot, *et al.*: *Phys. Rev. Lett.* **83** (1999) 840.
- 92) F. C. Zhang, C. Gros, T. M. Rice, and H. Shiba: *Supercond. Sci. Tech.* **1** (1988) 36.
- 93) K. -Y. Yang *et al.*: *Phys. Rev. B* **73** (2006) 224513.
- 94) A. Himeda and M. Ogata: *Phys. Rev. Lett.* **85** (2000) 4345.
- 95) T. Watanabe, H. Yokoyama, Y. Tanaka, and J. Inoue: *J. Mag. Mag. Mat.* **310** (2007) 648; Y. C. Chen: private communication.
- 96) H. Yokoyama and H. Shiba: *J. Phys. Soc. Jpn.* **67** (1987) 3582, and *J. Phys. Soc. Jpn.* **67** (1987) 3570.
- 97) W. H. Press, S. A. Teukolsky, W. T. Vetterling, and B. P. Flannery: *Numerical Recipes in FORTRAN, second ed.* (Cambridge, New York, 1992) p.406.
- 98) G. Zheng, P. L. Kuhns, A. P. Reyes, B. Liang, and C. T. Lin: *Phys. Rev. Lett.* **94** (2005) 047006.
- 99) D. Fournier *et al.*: *Nat. Phys.* **6** (2010) 905.
- 100) This function form does not correspond to that of a perturbation study of the BCS function for  $U \rightarrow 0$ :<sup>56)</sup>  $\Delta \propto \exp(-t^2/U^2)$ . Such a singular term should exist, but probably is dominant only for extremely small  $U$ .
- 101) As mentioned in ref. 16, total energies for  $U > U_{co}$  at half filling fit very well with  $-\gamma t^2/U$  ( $\gamma$ : const.), which corresponds to the result of strong coupling ( $t/U$ ) expansion.
- 102) Y. Yanase and M. Ogata: *J. Phys. Soc. Jpn.* **74** (2005) 064511.
- 103) P. F. Maldague: *Phys. Rev. B* **16** (1977) 2437.
- 104) See also, Y. Nagaoka: *Phys. Rev.* **147** (1966) 392.
- 105) As a recent review, M. Vojta: *Adv. Phys.* **58** (2009) 699.
- 106) For instance, M. Lugas, L. Spanu, F. Becca, and S. Sorella: *Phys. Rev. B* **74** (2006) 165122, and references therein.
- 107) C. -C. Chang and S. Zhang: *Phys. Rev. B* **78** (2008) 165101.
- 108) A. Paramekanti, M. Randeria, and N. Trivedi: *Phys. Rev. B* **70** (2004) 054504.
- 109) H. Kondo and T. Moriya: *J. Phys. Soc. Jpn.* **78** (2009) 013704.
- 110) Y. Suzumura, Y. Hasegawa, and H. Fukuyama: *J. Phys. Soc. Jpn.* **57** (1988) 401.
- 111) For instance, R. P. Feynman, *Statistical Mechanics* (Benjamin, Reading, 1972) Chap. 11.
- 112) J. W. Loram *et al.*: *J. Phys. Chem. Solids* **62** (2001) 59.
- 113) T. Matsuzaki *et al.*: *J. Phys. Soc. Jpn.* **73** (2004) 2232.
- 114) L. F. Tocchio, F. Becca, and C. Gros: *Phys. Rev. B* **83** (2011) 195138.
- 115) In a strict sense, hopping of a holon (or doublon) of a D-H pair is counted in  $E_h$  if the holon is separated by more than one lattice spacing from the partner doublon (in a process higher than second order). However, such a process occurs very rarely for large  $U/t$ 's, and may be neglected.<sup>20)</sup>
- 116) H. Takagi *et al.*: *Phys. Rev. Lett.* **69** (1992) 2975; S. Uchida *et al.*: *Phys. Rev. B* **43** (1991) 7942; N. Momono *et al.*: *Physica C* **233** (1994) 395; T. Yoshida *et al.*: *Phys. Rev. B* **74** (2006) 224510.
- 117) Y. J. Uemura, *et al.*: *Phys. Rev. Lett.* **66** (1991) 2665.
- 118) G. Xu *et al.*: *Nat. Phys.* **5** (2009) 642.
- 119) T. Watanabe *et al.*: *J. Phys. Chem. Solids* **67** (2006) 112.
- 120) M. Matsuda *et al.*: *Phys. Rev. B* **65** (2002) 134515.
- 121) M. Fujita *et al.*: *Phys. Rev. B* **67** (2003) 014514.
- 122) T. Watanabe, H. Yokoyama, Y. Tanaka, and J. Inoue: *Phys. Rev. B* **77** (2008) 214505.
- 123) K. Kobayashi and H. Yokoyama: *Physica C* **463-465** (2007) 141, and *J. Phys. Chem. Solids* **69** (2008) 3274.
- 124) Actually, it is not easy to optimize cases of  $t'/t = -0.4$ ,  $n = 0.80$ ,  $L = 10$  and  $10 \lesssim U/t \lesssim 20$ , because the variational energy becomes almost the same for  $0.05 \lesssim \Delta_d/t \lesssim 0.16$ , which yields  $0.002 \lesssim P_d^\infty \lesssim 0.015$ , suggesting that this parameter set is situated near the transition point. We refrain from using the data of this parameter set in the figures.
- 125) L. F. Tocchio, F. Becca, and C. Gros: unpublished (arXiv:1201.2298).
- 126) For instance, D. J. Scalapino, E. Loh Jr., and J. E. Hirsch: *Phys. Rev. B* **34** (1986) 8190; K. Miyake, S. Schmitt-Rink, and C. M. Varma: *Phys. Rev. B* **34** (1986) 6554.
- 127) S. R. White and D. J. Scalapino: *Phys. Rev. B* **60** (1999) R753.
- 128) G. B. Martins, J. C. Xavier, L. Arrachea, and E. Dagotto: *Phys. Rev. B* **64** (2001) 180513.
- 129) Although we use the bare band here, it is more appropriate to consider a renormalized band owing to the effect of  $U$ , which is a future problem.
- 130)  $n(\mathbf{k})$  seems stationary at  $(\pi, 0)$  at half filling, by inferring from the system-size dependence of  $|\nabla n(\mathbf{X}')|$  [see  $L$  in Fig. 31(e)]. For  $\delta \lesssim 0.05$ , owing to regular and large system-size dependence, the behavior of  $|\nabla n(\mathbf{X}')|$  for  $L = \infty$  is likely to resemble that of  $P_d^\infty$ .
- 131) M. Aichhorn, E. Arrigoni, Z. B. Huang, and W. Hanke: *Phys. Rev. Lett.* **99** (2007) 257002.
- 132) M. Civelli *et al.*: *Phys. Rev. Lett.* **100** (2008) 046402.
- 133) S. Sorella: *Phys. Rev. B* **64** (2001) 024512; C. J. Umrigar and C. Filippi: *Phys. Rev. Lett.* **94** (2005) 150201.
- 134) D. Tahara and M. Imada: *J. Phys. Soc. Jpn.* **77** (2008) 093703, and *J. Phys. Soc. Jpn.* **77** (2008) 114701.
- 135) P. Phillips: *Rev. Mod. Phys.* **82** (2010) 1719.
- 136) A. B. Harris and R. V. Lange, *Phys. Rev.* **157** (1967) 295; J. E. Hirsch: *Phys. Rev. Lett.* **54** (1985) 1317.
- 137) P. Fazekas, *Physica Scripta T* **29** (1989) 125.
- 138) In Table B-1, the energy of  $Q_j^S$  is unexpectedly close to that of an improved asymmetrized factor  $Q_j^{\text{DH}}$  even for  $n = 0.8$ . If we disregard the argument of D-H symmetry,  $Q_j^S$  may be used for  $n < 1$ . In this connection, we erroneously described in ref. 16 that  $Q_j^S$  does not work for  $n \neq 0$  and  $U > 0$ .
- 139) We adopt the stepwise or Manhattan metric to measure  $|\mathbf{r}|$ .



